

1 **Environmental responses to the 9.7 and 8.2 cold**  
2 **events at two ecotonal sites in the Dovre**  
3 **Mountains, Mid-Norway**

4 Aage Paus<sup>1</sup>, Hafliði Haflidason<sup>2</sup>, Joyanto Routh<sup>3</sup>, B. David A. Naafs<sup>4</sup>, and Mari W. Thoen<sup>1</sup>

5

6 <sup>1</sup>Department of Biological Science, University of Bergen, Post Box 7803, N-5020 Bergen,  
7 Norway

8 <sup>2</sup>Department of Earth Science, University of Bergen, Norway, and Bjerknes Centre for Climate  
9 Research, Norway

10 <sup>3</sup>Department of Thematic Studies – Environmental Change, Linköping University, Linköping  
11 58183, Sweden

12 <sup>4</sup>Organic Geochemistry Unit, School of Chemistry and Cabot Institute, University of Bristol,  
13 Bristol, UK

14

15 Corresponding author:

16 Aage Paus,

17 Telephone: + 47 55 58 33 44

18 Fax: + 47 55 58 96 67

19 E-mail: [aage.paus@uib.no](mailto:aage.paus@uib.no)

20

21 **Key words**

22 Early Holocene; Paleoclimatology; 9.7 and 8.2 cold events; Scandinavia; Lake  
23 sedimentology; Varves; Biomarkers; Vegetation dynamics; Ecotones

24

25 **Abstract**

26

27 We found strong signals of two cooling events around 9700 and 8200 cal yrs. BP in lakes  
28 Store Finnsjøen and Flåfattjønnå at Dovre, mid-Norway. Analyses included pollen in both  
29 lakes, and C/N-ratio, biomarkers (e.g. alkanes and br-GDGTs), and XRF scanning in  
30 Finnsjøen. The positions of these lakes close to ecotones (upper forest-lines of birch and pine,  
31 respectively) reduced their resilience to cold events causing vegetation regression at both  
32 sites. The global 8.2 event reflects the collapse of the Laurentide Ice Sheet. The 9.7 event with  
33 impact restricted to Scandinavia and traced by pollen at Dovre only, reflects the drainage of  
34 the Baltic Ancylus Lake. More detailed analysis in Finnsjøen shows that the events also  
35 caused increased allochthonous input (K, Ca), increased sedimentation rate, and decreased  
36 sediment density and aquatic production. br-GDGT-based temperatures indicate gradual  
37 cooling through the early Holocene. In Finnsjøen, ca. 3100 maxima-minima couplets in  
38 sediment density along the analyzed sequence of ca. 3100 calibrated years show the presence  
39 of varves for the first time in Norway. Impact of the 9.7 and 8.2 events lasted ca. 60 and 370  
40 years, respectively. Pine pollen percentages were halved and re-established in less than 60  
41 years, indicating the reduction of pine pollen production and not vegetative growth during the  
42 9.7 event. The local impact of the 8.2 event *sensu lato* (ca 8420 – 8050 cal yrs. BP) divides  
43 the event into a precursor, an erosional phase, and a recovery phase. At the onset of the  
44 erosional phase, summer temperatures increased.

45

46

## 47 **Introduction**

48

49 The early Holocene is characterized by a series of well-documented climate instabilities, i.e.  
50 cooling episodes, that are likely driven by a slow reorganization of the North Atlantic  
51 thermohaline circulation (e.g. Andersson et al., 2004; Berner et al., 2010; Wanner et al., 2011)

52 in combination with a decrease in summer solar insolation (Renssen et al., 2007) and probably  
53 also periodic presence of perennial Arctic sea ice cover (Stranne et al., 2014). The most  
54 prominent early Holocene cooling episodes ca. 11.300 cal yrs. BP (PreBoreal Oscillation:  
55 PBO), 9700-9300 cal yrs. BP (Erdalen 2 event *s.l.*), and 8200 cal yrs. BP (Finse event) are  
56 included in the quasi-periodic Holocene “Bond-cycles” (Bond et al., 1997). These climatic  
57 cycles are thought to be related to perturbations in solar radiation and/or continental ice sheet  
58 dynamics (Bond et al., 2001; Obrochta et al., 2016). The three cold periods are clearly  
59 recorded in the marine stratigraphy of the North Atlantic and Nordic Seas (e.g. Koç and  
60 Jansen, 1992; Haflidason *et al.*, 1995; Björck et al., 1997; Andersen et al., 2004; Berner et al.,  
61 2008, 2010), and by glacial deposits showing glacial readvances in Scandinavia and the Alps  
62 (e.g. Nesje and Dahl., 2001; Dahl et al. 2002; Bakke et al., 2005; Nicolussi and Schlüchter,  
63 2012; Gjerde et al., 2016; Moran et al., 2016).

64

65 The impact of these climatic events in Europe, and in particular, the impact on vegetation is  
66 less clear. Obviously, due to the remains of the decaying Weichselian Ice Sheet lingering, the  
67 records of the earliest climate oscillation are sparse in Scandinavia (Björck et al., 1997; Paus  
68 et al., 2015) compared to further south (Bos et al., 2007; Dormoy et al., 2009). In contrast, the  
69 influence on vegetation from the 8.2 event is more frequently recorded in mid- and northern  
70 Europe than southern parts of the continent (Ghilardi and O’Connell, 2013; Filoc et al., 2017).  
71 Nonetheless, well-established cases of this event have been identified in Spain (Davis and  
72 Stevenson, 2007), SE Europe (Budja, 2007), and as far east as Syria (van der Horn et al.,  
73 2015). Few studies document the 9.7-9.3 event, and those that do only show minor changes in  
74 vegetation (Wohlfarth et al., 2004; Whittington et al., 2015; Burjachs et al., 2016). In context  
75 of the distinct 9.7-9.3 signals recorded in marine sequences and glacial deposits, the lack of  
76 vegetation responses of similar strength and frequency in continental Europe is surprising as  
77 the underlying mechanism is thought to be the same for all events. A possible cause for the

78 fragmented records could be low sample resolution at some sites (Whittington et al., 2015),  
79 but most probably, the lack of studies at ecotonal sites could explain the limited vegetation  
80 signal for this event. It is at the vegetation boundaries, the ecotones, that vegetation is less  
81 resilient to climate change (Smith, 1965; Fægri and Iversen, 1989), and here the strongest  
82 effects of cold events are signaled. Today, numerical treatments of large pollen-data sets find  
83 regional patterns of vegetation and climate change (e.g. Seppä et al., 2007; Seddon et al.,  
84 2015; Hjelle et al., 2018). However, the number of sites may not be crucial for elaborating  
85 detailed geographical patterns of these events. More important is the quality of sites studied  
86 including their ecotonal positions.

87

88 This study compares multi-proxy records from two sites at Dovre (Norway): Flåfattjønna (Paus,  
89 2010) and Finnsjøen, where the pollen data are reported by Thoen (2016). The aim is to shed  
90 new light on the question whether the early Holocene “Bond”-events impacted climate and  
91 vegetation in northern Europe. The lakes were close to ecotones (Flåfattjønna: upper pine-forest  
92 line, Finnsjøen: upper birch-forest line) during the Early Holocene, and show two short-lasting  
93 vegetation fluctuations during this period. To investigate the causes of these climatic  
94 oscillations, we use AMS-dates of terrestrial macrofossils and principle component analysis  
95 (PCA) of the Finnsjøen and Flåfattjønna pollen data, combined with XRF-scanning, elemental  
96 (C/N) ratio, and biomarker (glycerol diacyl glycerol tetraethers (GDGT) and *n*-alkane)  
97 analyses.

98

## 99 **2. Regional setting**

100

101 The Dovre mountain ridge with Lake Store Finnsjøen is situated between the valleys Drivdalen  
102 and Vinstradalen in Oppdal, Trøndelag County (Norway) (Fig. 1). Lake Flåfattjønna lies 30 km  
103 to the east of the ridge, in Tynset, Hedmark County (Fig. 1 and Paus et al., 2006; Paus 2010).

104 Features of the two lakes and their surroundings are listed in Table 1. In continental areas such  
105 as the study area, the birch-forest line roughly follows the 10 °C July isotherm (Odland, 1996).  
106 Both lakes lie in the low alpine zone characterized by lichen-dominated dwarf-shrub tundra. In  
107 Drivdalen, 2 km west of Finnsjøen (Fig. 1), birch-forests reach ca. 1100 m a.s.l., and pine-  
108 forests ca. 900 m a.s.l. The region including Finnsjøen is renowned for its well-developed and  
109 species-rich flora that includes plants with a so-called centric distribution in Scandinavia. More  
110 details regarding environmental features of these sites are included in Paus et al. (2006, 2015)  
111 and Paus (2010).

112

113

### 114 **3. Material and methods**

115

116 We refer to Paus et al. (2006) and Paus (2010) for details on material and methods of the  
117 Flåfattjønn study. The Finnsjøen material and methods are described below.

118

#### 119 *3.1. Sampling and lithostratigraphy*

120 The Finnsjøen lake sediments were cored at maximum water depth (14.7 m) from the ice-  
121 covered lake surface during winter. A 110-mm piston corer (Nesje, 1992) modified by A. Paus  
122 and J. Kusior (Dept. of Earth Science, Univ. of Bergen) was applied, which allowed us to use  
123 6-m tubes and start sampling maximum 5 meters below the sediment surface. In Paus et al.  
124 (2015), results from the core section 1980-2195 cm below water surface were reported. The  
125 more detailed Holocene results presented in this paper, are based on the core section 1865-2040  
126 cm depth below water surface showing distinctly laminated gyttja with numerous macrofossil  
127 and/or silty layers (Fig. 2). The analyzed sediments were described (Table 2) according to the  
128 method by Troels-Smith (1955). Sediments were cored in one continuous sequence. Hiati or  
129 correlated overlaps are absent in the core. However, during the XRF logging that requires length

130 of sections less than 180 cm, one core section was cut one cm too long. Hence, 1 cm (2015-  
131 2014 cm depth below water surface) was removed from one core section. This 1 cm gap is  
132 shown as hiatus in Fig. 2.

133

### 134 *3.2. Geochemical core logging*

135 The loss-on-ignition (LOI) was measured in levels at 1-10 cm intervals in the studied core  
136 section. The sub-samples were dried overnight at 105 °C, weighed and ignited at 550 °C for 1  
137 h. LOI was calculated as percentages of dry weight.

138

139 To document the sediment structure in the minerogenic part of the core, sediments were X-ray  
140 photographed using a Philips X-ray 130 kV instrument. The X-ray imagery was processed on  
141 a negative film, and thereafter transferred into a positive format using a digital camera. The  
142 resulting photos are found in Figs. 2 and 7.

143

144 The non-destructive ITRAX  $\mu$ XRF element core scanner from Cox Analytical Systems was applied to  
145 analyze variations in geochemical properties along the core surface as well as the colour- and the X-  
146 ray imaging. The core was scanned using a molybdenum (Mo) tube with a downcore resolution of 200  
147  $\mu$ m. The voltage and current were set to 35 kV and 50 mA, respectively, with a counting time of 10 s  
148 for each analytical step. The elements selected to represent downcore lithological variations are  
149 potassium (K) and calcium (Ca). In addition to elemental and colour scans of the core surface, a  
150 density graph was extracted from X-ray images and plotted versus depth with the same resolution like  
151 elemental analyses. Because X-rays penetrate through the core, they represent density and illustrate  
152 the overall layering that characterizes the sediment record.

153

### 154 *3.3 Radiocarbon dating, varves and age-depth modelling*

155 Eleven samples of terrestrial plant remains from the Finnsjøen sediments between 1810 and  
156 2055 cm depth below water surface were AMS radiocarbon-dated (Table 3). All dates were  
157 reported as calibrated years BP (cal yrs. BP; present = AD 1950) based on the InCal13  
158 calibration curve (Reimer et al. 2013). We converted the dates to calendar ages using CALIB  
159 7.10 (Stuiver et al., 2017). The age-depth modelling (Fig. 3a) was obtained with the CLAM  
160 2.2 R package (Blaauw, 2010) which recognized two outliers. The small variations in  
161 sedimentation rates displayed in Fig. 3a most likely reflect dating inaccuracies. When  
162 estimating pollen accumulation rates (PAR) and plotting different sedimentary features versus  
163 age (Figs. 2, 4, 5, and 7), we used the linear sedimentation rate estimated by interpolating  
164 between the oldest and youngest dates.

165

166 When Figs. 2 and 7 were enlarged, a microscale pattern of the XRF density graph and the Ca  
167 and K curves appeared showing couplets of alternating maxima and minima. For the density  
168 graph, we counted ca. 3100 couplets in the analysed sediment sequence spanning ca. 3100  
169 calibrated years, which indicates the presence of annual varves (see discussion in section 4.1).  
170 However, the density curve reflected a floating chronology with no fixed attachment points to  
171 the radiocarbon chronology (Fig. 3b). Only minor differences were noted between the two  
172 chronologies. We have chosen to use the radiocarbon chronology to date the onset of events  
173 and estimating the sedimentation rates. On the other hand, the varve chronology was used to  
174 estimate the duration of events.

175

### 176 *3.4. Pollen*

177 Material for pollen analysis was sampled at 0.5–15 cm intervals between 1865 and 2040 cm  
178 depth. The samples were treated with HF and acetolysed according to Fægri and Iversen  
179 (1989). We added *Lycopodium* tablets to the samples (1 cm<sup>3</sup>) for estimates of concentration  
180 and pollen accumulation rates (PAR; Stockmarr, 1971). Identifications were based on Fægri

181 and Iversen (1989), Moore et al. (1991), and Punt et al. (1976-1996) in combination with a  
182 reference collection of modern material at University of Bergen. *Betula nana* pollen was  
183 distinguished using the morphological criteria of Terasmäe (1951). The pollen diagrams  
184 (Figs. 4, 5, and 6) were drawn by the computer program CORE 2.0 (Kaland and Natvig,  
185 1993). In the pollen percentage diagram (Fig. 6), the calculation basis ( $\Sigma P$ ) comprised the  
186 terrestrial pollen taxa. For taxon X of aquatic plants (AQP) and spores, the calculation basis  
187 was  $\Sigma P+X$ . We used the computer program CANOCO 4.5 (ter Braak and Smilauer, 1997-  
188 2002) for detecting and plotting ordination patterns in the terrestrial vegetation development.  
189 The analysed data set included results from Lake Store Finnsjøen merged (using the option in  
190 CORE 2.0) with pollen results from the same time interval (7600-10.700 cal yrs. BP) in  
191 sediments of Lake Flåfattjøenna, ca. 30 km east of Lake Finnsjøen (Paus, 2010; Paus et al.,  
192 2006).

193

194 Palynological terrestrial richness (PR) was estimated by rarefaction analyses (program  
195 RAREPOLL, Birks and Line, 1992) using the minimum sum of terrestrial microfossils (= 565)  
196 as the statistical base ( $E(T_{565})$ ). Intermediate levels of disturbance maximize richness by  
197 preventing both dominance and extinction of species (Grime, 1973). In accordance with this,  
198 the low estimated terrestrial PR  $E(T_{565})$  for abundant tree pollen (AP) (Fig. 4) should indicate  
199 closed forests, whereas local PR maxima indicated periods when the vegetation was positioned  
200 close to and above the forest-line (e.g. Aario, 1940; Simonsen, 1980; Seppä, 1998; Grytnes,  
201 2003). However, at Finnsjøen pine-pollen was not a local signal (see section. 5.2.). To estimate  
202 local changes in palynological richness at Finnsjøen, we also estimated palynological richness  
203 ( $E(T_{102})$ ) by subtracting the dominant regional pine pollen from the statistical basis (Fig. 4).

204

205 *3.5. Biochemical characterisation*



206 C/N analyses: The lake sediments were freeze-dried for 48 hrs to remove all traces of water.  
207 The freeze-dried samples were kept in a desiccator with 12M HCl (48 hours) to remove any  
208 traces of carbonates present in the sediments (Hedges and Stern, 1984). Elemental C and N  
209 were measured on a Perkin Elemental analyzer (2400 series II CHNS/O) for specific lake  
210 samples together with certified standards (Jet Rock, Svalvard Rock). The reproducibility of  
211 elemental analysis was  $\pm 10\%$ .

212  
213 Lipids: Plant waxes were extracted from ca. 1-4 g of freeze-dried sediment from selected  
214 intervals (see Fig. 2) with a mixture of dichloromethane and methanol (ratio of 9:1 by  
215 volume) by an automated solvent extraction (Dionex ASE 300). The total lipid extracts were  
216 injected into an Agilent 6890 gas chromatograph with a HP5-MS column (30 m  $\times$  0.25 mm  
217 internal diameter  $\times$  0.25  $\mu\text{m}$  film). The oven temperature was kept constant at 35°C for 6  
218 minutes, increased to 300 °C at 5 °C min<sup>-1</sup> and then held for 20 minutes. The chromatograph  
219 was coupled with an Agilent 5973 mass spectrometer and operated at 70 eV to scan the full  
220 range of charged particles from m/z 50 to 600 amu. High purity standards (S-4066) from  
221 Chiron (Trondheim, Norway) and deuterated compounds from Sigma-Aldrich (Munich,  
222 Germany) were used for quantification. The total input of higher odd *n*-alkane concentrations  
223 (*n*-C<sub>27</sub>, C<sub>29</sub> and C<sub>31</sub>) was used to calculate the input of terrestrial plant waxes derived from  
224 higher plants. In addition, the ratio P<sub>aq</sub> (Ficken et al. 2000) was calculated to estimate the  
225 input of waxes derived from in-lake algal production

226

227

228

$$P_{\text{aq}} = \frac{C_{23} + C_{25}}{C_{23} + C_{25} + C_{29} + C_{31}}$$

229

230 where C<sub>n</sub> refers to *n*-alkane carbon chain length.

231

232 Glycerol dialkyl glycerol tetraether (GDGT): The total lipid extract of 11 of the Finnsjøen  
233 samples was re-dissolved in hexane/*iso*-propanol (99:1, v/v) and filtered using 0.45 µm PTFE  
234 filters. The branched and isoprenoidal GDGT distribution was analysed by high performance  
235 liquid chromatography/atmospheric pressure chemical ionisation – mass spectrometry  
236 (HPLC/APCI-MS) using a ThermoFisher Scientific Accela Quantum Access triple  
237 quadrupole MS. Normal phase separation was achieved using the method of Hopmans et al.  
238 (2016) that consists of two ultra-high performance liquid chromatography silica columns in  
239 tandem. Injection volume was 15 µL from 300 µL. To increase the sensitivity and  
240 reproducibility, all analyses were performed using the selective ion monitoring mode (SIM) to  
241 detect specific ions (*m/z* 1302, 1300, 1298, 1296, 1294, 1292, 1050, 1048, 1046, 1036, 1034,  
242 1032, 1022, 1020, 1018, 744, and 653).

243 The relative abundance of 6-methyl over 5-methyl br-GDGTs is expressed as the IR<sub>6me</sub> ratio  
244 (De Jonge et al., 2013).

245

$$IR_{6me} = \frac{IIa' + IIb' + IIc' + IIIa' + IIIb' + IIIc'}{IIa + IIa' + IIb + IIb' + IIc + IIc' + IIIa + IIIa' + IIIb + IIIb' + IIIc + IIIc'}$$

246

247 In addition, the branched versus isoprenoidal tetraether (BIT) index (Hopmans et al., 2004)  
248 that reflects the relative abundance of the major bacterial br-GDGTs versus crenarchaeol, an  
249 iso-GDGT likely produced exclusively by *Thaumarchaeota* (Sinninghe Damsté et al., 2002),  
250 was also quantified

251

$$BIT = \frac{(Ia + IIa + IIa' + IIIa + IIIa')}{(Ia + IIa + IIa' + IIIa + IIIa' + crenarchaeol)}$$

252

253

254 **4. Results**

255

256 *4.1. Lithostratigraphy*

257 The sedimentation rate appears approximately linear showing an average growth of 0.56 mm/  
258 year (or 17.7 years/cm) in the studied time interval 10.700-7600 cal yrs. BP (Fig. 3a). The core  
259 section 1865-2040 cm below the water surface consists of distinctly laminated to sub-laminated  
260 gyttja as indicated by the high-resolution colour scan and the density graph plot. The lamina  
261 observed by eye (Figs. 2 and 7) are normally 0.5-0.6 mm thick and occur as greyish silty  
262 horizons or as darker layers of distinct concentrations (amount) of macrofossils. The variability  
263 in the density graph also shows the laminated structure of the core confirming that the  
264 lamination is not only preserved in the top layer of the core, but is the structure of the entire  
265 core. Down-core density is plotted versus the number of electrons penetrating the core section  
266 for every 200  $\mu\text{m}$ . The lower the cps number is, the higher the density. And the higher sediment  
267 density is, the higher minerogenic content in the core. The shift from minerogenic sediments to  
268 an increasing amount of biogenic components is clearly shown at ca. 10350 cal yrs. BP. The  
269 shift at 9800 cal yrs. BP to lower sediment density (higher cps) reflects transfer to a period with  
270 increased biogenic production and content. These depositional conditions dominated by higher  
271 biogenic production, characterise the period studied in this core. It is punctuated by short  
272 periods of increased minerogenic content, composed of higher density and/or lower  
273 productivity, centred around 9650, 9340 and 8200 cal yrs. BP (Figs. 2 and 7). Similarly, the  
274 relative concentration of potassium (K) and calcium (Ca) reflects the lithological variability  
275 with similar amplitude as expressed in the density graph. These lithological variations around  
276 the postulated cool periods are consistent with colour imaging indicating distinct shifts in  
277 colour. Notably, the lamina appear coarser and thicker than the warm periods (Figs 2 and 7).  
278 Because K and Ca represent particles from the local bedrock, the variability measured reflects  
279 shifts in allochthonous contributions. The major increases of K and Ca around cooling periods

280 is centred around 9650 and 8200 cal yrs. BP and illustrates the sensitivity of this parameter to  
281 local environmental changes.

282 The lithostratigraphy also shows microscale laminations superimposed on the laminations  
283 observed by eye. Both for sediment density and the elements K and Ca there are densely shifting  
284 values where maxima alternate with minima forming couplets (Figs. 2 and 7). We counted 3117  
285 density couplets over the 3100 calibrated years spanned by the analysed Finnsjøen sediments.  
286 This strongly points to the deposition of annual varves in Finnsjøen, here reported for the first  
287 time in Norway. The density maxima (i.e. low cps) reflect increased allochthonous minerogenic  
288 input during the thawing in spring/early summer, whereas the density minima (i.e. high cps)  
289 represent autochthonous organic production during summers (consistent with lower C/N and  
290 terrestrial organic matter input albeit representing low-resolution measurements). Hence, the  
291 varve origin appears as a mixture of clastic and biogenic factors (Zolitschka et al., 2015).

292 The clear-cut changes in K and Ca concentrations at the lower boundary of the 9.7 and the 8.2  
293 cooling events are interpreted to represent gaps of 1.1–1.5 cm of the lake record due to climate  
294 influenced erosion of the underlying laminated units. These estimates are based on the counting  
295 and thickness estimates of lamina compared with the age model (Fig. 3a). The gaps are  
296 calculated to represent a removal of maximum 12 years of sediments at the beginning of the 9.7  
297 event and maximum 20 years of sediments at the beginning of the 8.2 event. Obviously, this  
298 reflects a source of error for establishing a reliable varve chronology.

299

#### 300 *4.2. Pollen results and statistical analysis*

301 We identified 47 terrestrial taxa in 47 levels of the Finnsjøen sediment-section. The pollen sum  
302 of terrestrial taxa analysed per sample varied between 535 and 2066 (mean  $\Sigma P$ : 1035). Seven  
303 local pollen assemblage zones were defined by visual inspection (Figs. 2, 5 and 6, Table 4). In

304 five PAZ (S-2 to S-6), pine dominates showing values of 40-90%  $\Sigma$ P. During this period of pine  
305 maximum, there are two distinct and short-lasting pine minima of 40-50%  $\Sigma$ P (PAZ S-3 and S-  
306 5). At the same time, *Betula*, *Juniperus* and algae show percentage maxima.

307

308 The merged data set from lakes Finnsjøen and Flåfattjøenna was subjected to a DCA  
309 ordination that showed a gradient length of 1.70 SD. This suggested linear response curves.  
310 Hence, we chose PCA as an ordination technique. A preliminary PCA including the dominant  
311 and entirely regionally represented *Pinus* (see section 5.2.), condensed scatter plots, and axis  
312 1 captured 62% of the variation in the data. To reduce the influence of pine and enhance the  
313 influence of local features, pine was included as passive in the PCA (Figs. 8 and 9).

314 Palynological richness (PR) and LOI were added as environmental variables during the  
315 statistical assessment. In Fig. 8, the light-demanding pioneers are concentrated to the left with  
316 medium to low axis 2 values, along with PR. Deciduous trees (e.g. *Ulmus*, *Corylus*) and herbs  
317 (e.g. *Valeriana*, *Geranium*) on fertile soils are situated to the right and/or at high axis 2  
318 values. *Pinus* and LOI occur to the extreme right.

319

#### 320 4.3. Biochemical results

321 C/N ratio varies between 12-20 indicating inputs of lacustrine algal production and higher  
322 plants from the catchment typical of lacustrine environments (Das et al., 2008). Higher values  
323 coincide with the onset of the cold 9.7 and 8.2 events due to soil erosion and increased outwash  
324 of nutrients, before it declines with the intensification of colder temperatures. C/N gradually  
325 increases after the cold periods. This transition is most evident after the 8.2 event.

326

327 *n*-Alkane concentrations increase core upwards with inflection points coinciding with the 9.7  
328 and 8.2 cooling events (Fig. 2), interpreted as terrestrial organic matter and aquatic input. A  
329 lower  $P_{aq}$  ratio suggests less algal productivity. The percentage of terrestrial organic matter

330 (mainly plant waxes) declines sharply by nearly 20% after the onset of the cold events and  
331 recovers again after climate ameliorates and vegetation recovers in the catchment. The increase  
332 of terrestrial organic matter is larger during the post-9.7 warming than during the recovery after  
333 the 8.2 event.

334

335 Glycerol dialkyl glycerol tetraethers (GDGTs) are abundant biomarkers in most types of  
336 natural archives (Schouten et al., 2000; Schouten et al., 2013). Two types of main GDGTs are  
337 recognized; Archaea synthesize isoprenoidal (iso-GDGTs), whereas bacteria synthesize  
338 branched (br-GDGTs) compounds. In general, br-GDGTs are more abundant in terrestrial  
339 settings, whereas iso-GDGTs are more abundant in sediments from large lakes and marine  
340 environments (Hopmans et al., 2004). Iso-GDGTs can have between 0 and 8 cyclopentane  
341 rings, whereas crenarchaeol has four cyclopentane and one cyclohexane ring (De Rosa and  
342 Gambacorta, 1988; Schouten et al., 2000; Sinninghe Damsté et al., 2002; Schouten et al.,  
343 2013). br-GDGTs can have between 0 and 2 cyclopentane rings and/or between 0 and 2  
344 additional methyl groups at either the C5 and C6 position ( De Jonge et al., 2013; Schouten et  
345 al., 2000, 2013; Sinninghe Damsté et al., 2000).

346

347 In mineral soils, peat, and lake sediments, the degree of methylation of br-GDGTs is  
348 correlated with mean annual air temperature (MAT), while the degree of cyclization of br-  
349 GDGTs and the relative abundance of 6-methyl br-GDGTs over 5-methyl br-GDGTs is  
350 correlated with the pH (e.g., Weijers et al., 2007; Loomis et al., 2012; De Jonge et al., 2014;  
351 Naafs et al., 2017; Russell et al., 2018).

352

353 In all 11 samples from Finnsjøen, taken between 2022 and 1870 cm below water depth,  
354 GDGTs were present in abundance. The GDGT distribution was dominated by bacterial br-  
355 GDGTs over archaeal iso-GDGTs. The dominant archaeal lipid was iso-GDGT-0 with a

356 relative abundance over iso-GDGT-1, -2, and -3 above 90%. Crenarchaeol was present in low  
357 abundance and the BIT index, reflecting the ratio between br-GDGTs and crenarchaeol,  
358 varied between 0.98 and 1.00. The br-GDGTs were dominated by acyclic 5-methyl  
359 homologues Ia, IIa, and IIIa with the latter being the most abundant compound with a relative  
360 abundance over all br-GDGTs of ~ 30%. In all samples, 5-methyl br-GDGTs were the most  
361 abundant, but 6-methyl br-GDGTs were also present. The IR<sub>6me</sub> ratio, reflecting the ratio  
362 between 6- and 5-methyl br-GDGTs, ranged from 0.3 to 0.4.

363

364 The dominance of br-GDGT over iso-GDGTs, the small size of the lake, as well as the  
365 broader biomarker distribution (see above) suggests that the majority of GDGTs are derived  
366 from the surrounding soils. As such we used the global mineral-soil based calibration to  
367 convert the br-GDGT distributions into temperature and pH estimates (De Jonge et al., 2014).

368

$$369 \quad MAT_{mr} (\text{°C}) = 7.17 + 17.1 \times \{Ia\} + 25.9 \times \{Ib\} + 3.44 \times \{Ic\} \\ -28.6 \times \{IIa\} \quad (\text{RMSE} = 0.46 \text{ °C})$$

370

$$371 \quad pH = 7.15 + 1.59 \times CBT' \quad (\text{RMSE} = 0.52)$$

372

$$373 \quad CBT' = \log \frac{(Ic + IIa' + IIb' + IIc' + IIIa' + IIIb' + IIIc')}{(Ia + IIa + IIIa)}$$

374

374

375 The MAT<sub>mr</sub>-based temperatures range between 3 and 6 ± 4.6 °C. Temperatures gradually  
376 decrease along the core with highest temperatures recorded in the oldest samples. The pH was  
377 relatively constant around 6.5 and mimics the temperature decline with slightly higher pH  
378 values in the oldest samples (Fig. 2).

379

## 380 **5. Discussion**

381

382 5.1. Background climate

383 The low-resolution biomarker data based on *n*-alkanes and br-GDGT provides  
384 complementary information about the organic matter sources and how the changes were  
385 driven by climate fluctuations.

386

387 The br-GDGT based terrestrial temperatures ( $MAT_{mr}$ ) from Finnsjøen (Fig. 2) provide a  
388 general context of background climate in the region on which the “Bond”-events are  
389 superimposed. We explicitly assume that 1) br-GDGTs in the mineral soils surrounding the  
390 lake are the main source of these compounds accumulating in the lake sediments, and 2) br-  
391 GDGT distribution is biased towards the warmer season. It is hard to confirm these  
392 assumptions, but given that we do not detect the novel hexamethylated GDGT only known  
393 from lacustrine production (Weber et al., 2015), the small size of the lake, abundant presence  
394 of higher plant waxes and elevated C/N values, it is likely that most of the organic matter in  
395 the lake sediments is not derived from *in situ* production in the lake. At present, the region  
396 experiences temperatures well below freezing during winter months with average  
397 temperatures in January around -11.5 °C (Table 1). Temperatures are on average 7.5 °C in  
398 July. It is not clear whether br-GDGTs in soils that experience <0 °C temperatures during part  
399 of the year are predominantly produced during the warmer season (Peterse et al., 2009;  
400 Weijers et al., 2011; Deng et al., 2016), but as bacterial growth is temperature dependent, it is  
401 likely that production of br-GDGTs in top soils is dominated by production when  
402 temperatures are above freezing, before being washed into the lake. The reconstructed  
403 temperatures for the early Holocene between 3 and  $6 \pm 4.6$  °C are 5 to 8 °C higher than  
404 present-day annual mean temperatures of -2.5 °C, further supporting a bias in br-GDGT  
405 production to periods when temperatures are above freezing. For comparison, the average of  
406 mean monthly temperatures above zero is today estimated to 3.5 to 4 °C at the altitude of  
407 Finnsjøen. The temperature evolution with ~2 °C higher  $MAT_{mr}$  around 10.000 cal yrs. BP



408 compared to 8000 cal yrs. BP, follows the local summer insolation pattern (Fig. 2), providing  
409 additional evidence that the record is biased towards the warm season. Thus, it does not  
410 represent the annual mean temperatures. Our data supports the hypothesis that the Holocene  
411 thermal maximum (HTM) in Scandinavia occurred during the early Holocene, and may have  
412 occurred earlier than the pine maximum in this region.

413

414 The MAT<sub>mr</sub> calibration error of  $\pm 4.6$  °C and sample resolution prevent the identification of  
415 Bond-events in the temperature record. However, MAT<sub>mr</sub> does provide information about the  
416 regional background climate, which was a few degrees C warmer than at present. This is  
417 consistent with palaeobotanical records from southern Scandes Mountains (Kullman, 2013;  
418 Paus, 2013; Paus & Haugland, 2017).

419

## 420 *5.2. Regional pine pollen*

421 The period in focus includes the Early Holocene pine maximum that is distinctly displayed in  
422 pollen diagrams from alpine areas in South-Scandinavia (e.g. Bergman et al., 2005; Bjune,  
423 2005; Gunnarsdottir, 1996; Velle et al., 2005, Segerström and Stedingk, 2003). During this  
424 pine maximum, numerous megafossils show that the pine-forests reached their maximum  
425 elevation in south-Scandinavia (Selsing, 1998; Kullman, 2013; Paus and Haugland, 2017).

426 These pine forests perhaps never reached much higher than 1105-1110 m a.s.l. in the study  
427 area because no megafossils are found above this elevation (Paus, 2010; Paus et al., 2011).

428 According to Paus & Haugland (2017), pine-forests did not reach more than ca. 250 m higher  
429 than present forests during the pine maximum. This would imply an early Holocene pine  
430 forest-line at ca. 1150 m a.s.l. at Dovre, which is ca. 100 m lower than the altitude of  
431 Finnsjøen. Pollen and macrofossil data from Råtåsjøen (1169 m a.s.l.), ca. 16 km SSE of  
432 Finnsjøen, supports this conclusion (Velle et al. 2005).

433

434 On the other hand, the pine sedaDNA (Paus et al., 2015), the extremely high pine PAR (45  
435  $10^3$  grains  $\text{cm}^{-2} \text{a}^{-1}$ ), and the high pine pollen percentages (90 %  $\Sigma\text{P}$ ) in sediments of Finnsjøen  
436 (1260 m a.s.l.) could contradict this conclusion. We regard these evidences of local pine  
437 forests as doubtful based on the following arguments. Pine sedaDNA was only found in one  
438 core-interval (Paus et al., 2015) which could reflect long-distance transport of pine remains or  
439 single specimens of low-growing “Krumholz” pine that are currently found up to 1200 m  
440 a.s.l. at Dovre. The PAR values are ca. 40 times higher than the threshold for indicating local  
441 pine forests (Jensen et al.; 2007; Seppä and Hicks, 2006) and reflect extreme sediment  
442 focusing (Davis et al., 1984; see discussion in Paus et al., 2015). Lastly, lowland hillsides in  
443 Drivdalen (Fig. 1) where tree-birch and pine grow today, would have been important sources  
444 for long-distance pollen. Such pollen could be dominant when local pollen production was  
445 low. Moreover, it is macrofossils of *Betula pubescens* and not pine that are found in the  
446 Finnsjøen sediments (Table 3) indicating presence of birch-forests in adjacent areas. The pine  
447 derived pollen is nevertheless dominant in the lacustrine record. Perhaps the birch-forests  
448 were open and had low pollen-production. Hence, the representation of long-distance pine  
449 pollen was enhanced in the sedimentary record. It is well known that pine is represented by  
450 dominant long-distance transport in other pollen based studies from the Arctic-Alpine regions  
451 (Aario, 1940; Gajewski, 1995; Paus, 2000). With these interpretative constraints on the pine  
452 pollen signal, we reconstruct the following local vegetation and climate development for the  
453 Finnsjøen area.

454

### 455 *5.3. General trends of local vegetation development*

456 The PCA ordination (Figs. 8, 9) roughly displays gradients of vegetation density/soil  
457 thickness increasing towards the right (axis 1) and soil fertility increasing upwards (axis 2).  
458 At Finnsjøen, pollen from *Pinus* and the warmth-demanding *Corylus*, *Ulmus*, and *Quercus*  
459 shows the strong influence of long-distance pollen transport. Nevertheless, local successions

460 can be distinguished. Species-diverse pioneer vegetation on shallow soils developed (PAZ S-  
461 1; lower left in Figs. 8, 9), and is followed by forests with *Betula pubescens*, *Populus tremula*,  
462 and (from 9300 cal yrs. BP) *Alnus incana* on more organic-rich soils (PAZ S-2 to S-6).  
463 Thereafter, tall-herb *Betula/Sorbus/Alnus* forests with e.g. *Valeriana*, *Geranium*, *Filipendula*,  
464 and *Urtica*, developed on the fertile soils in protected sites locally, whereas dwarf-shrub  
465 heaths expanded on wind-exposed ridges (PAZ S-7).

466

467 Within the same period (7600-10.700 cal yrs. BP), the local development at Flåfattjønn  
468 followed a similar pattern (Paus, 2010), but deviated chronologically in some successional  
469 stages. First, Flåfattjønn was deglaciated more than 800 years later than Finnsjøen (Paus et  
470 al., 2015), and therefore showed a lagged succession by a delay in leaching of soil minerals  
471 into the lake. Fig. 9 shows that pioneer plant communities on unweathered mineral-soils (PAZ  
472 F-2) developed ca. 10.700 cal yrs. BP at Flåfattjønn; a successional stage that was reached  
473 earlier at Finnsjøen (Paus et al., 2015). However, even if weathering and leaching of soils  
474 started just after local deglaciation, soil pH was still high at Finnsjøen in PAZ S-1 (Fig. 2).  
475 Second, even if pine-forests thrived at Flåfattjønn (1110 m a.s.l.) and did not at Finnsjøen  
476 (1260 m a.s.l.), the pollen record showed maximum pine values for a longer period at  
477 Finnsjøen (ca 10.000 – 8000 cal yrs. BP) compared to Flåfattjønn (9700 – 8500 cal yrs. BP;  
478 Fig. 4). It is likely that Drivdalen (2 km west of Finnsjøen and 700 m a.s.l.; Fig. 1), where  
479 temperatures allowed pine to grow for a longer period than at higher elevations, was an  
480 important contributor to the regional pollen representation at Finnsjøen. This would result in a  
481 stronger and longer-lasting percentage signal at the high-altitude Finnsjøen with vegetation of  
482 lower local pollen production than at Flåfattjønn (cf. Aario, 1940; Ertl et al., 2012).

483

484 During the pine maximum, when Finnsjøen was situated close to the upper birch-forest  
485 ecotone, and Flåfattjønn was situated close the upper pine-forest ecotone, the two distinct

486 episodes of reduced pine percentages occur around 9700 cal yrs. BP and 8400-8200 cal yrs.  
487 BP at both Finnsjøen and Flåfattjønnen (Fig. 4).

488

#### 489 5.4. The 9.7 cold event – Erdalen event 2

490 Around 9700-9600 cal yrs. BP in the Finnsjøen sediments, pine percentages, pine PAR, and  
491 LOI (Figs. 2, 4, 5 and 6) reach short-lasting minima, K and Ca element intensity and X-ray  
492 density (Fig. 2) reflect increased soil erosion and outwash resulting in increased lamina  
493 thickness, whereas *n*-alkanes show lowered input of both terrestrial organic matter and  
494 aquatic homologs (Fig. 2). The short-lasting C/N maximum is interpreted to reflect erosion  
495 and outwash of terrestrial organic matter, whereas declining C/N values show that colder  
496 conditions reduced terrestrial input more than the aquatic production (cf. alkanes of terrestrial  
497 organic matter vs.  $P_{aq}$ ). The first part of the subsequent C/N rise reflects lower aquatic  
498 production, whereas the later rise shows a warming that increased the terrestrial input more  
499 than the aquatic production according to the *n*-alkane trends.

500

501 In PAZ S-3 of the Finnsjøen pollen diagram, constituting the three-level pine percentage  
502 minimum (Fig. 6), PAR values of *Betula*, *Juniperus*, and *Salix* show little change from the  
503 previous S-2 (Fig. 5). Hence, their S-3 percentage maxima reflect the reduction of pine  
504 entirely represented by regional/long-distance pollen (see section 5.2.). In addition, after  
505 removing regional pine from the calculation basis, palynological richness shows no distinct  
506 changes (Fig. 4). However, PCA with pine removed from the data set, shows that the local S-  
507 3 vegetation returned towards previous pioneer stages of S-1 (Fig. 9). Altogether, the  
508 stratigraphical trends indicate the 9.7 changes as a cold event that influenced lacustrine and  
509 terrestrial productivity. However, the GDGT temperature estimates show no distinct changes  
510 (see section 5.1).

511

512 The onset of the 9.7 cold event is signaled by both regional (i.e. decline in pine) and local  
513 (e.g. Ca and C/N increase) parameters. The floating varve chronology (see section 4.1)  
514 suggests that LOI decreased ca. 10 years later than pine. This delayed LOI decrease might  
515 reflect the time needed to erode top soil within the lake's catchment. The soil-independent  
516 algae (cf. *Pediastrum*) took advantage of nutrients washed out during the cold event. They  
517 flourished around the same time as regional pine abruptly increased (Figs 2, 5 and 6) both  
518 trends support the onset of climate warming during this period. Local vegetation regrowth and  
519 soil formation, shown by increasing LOI, lagged climate amelioration by 10-15 years  
520 according to the varve chronology. The upper boundary of the dark eroded layer occurs when  
521 LOI reached pre-9.7 values.

522

523 According to the floating varve chronology (Figs. 3b, 7), the impact of the 9.7 cold event  
524 lasted ca. 56-58 years. Increased soil erosion and outwash during the event seem to have  
525 increased varve thickness above the average sedimentation rate of 0.56 mm/yr to a rate of ca.  
526 0.77 mm/yr. Accordingly, the influence on regional pine lasted for ca. 56-58 years before pine  
527 pollen production recovered. Missing sediments from this section could add maximum 12  
528 years to the duration of the 9.7 impact (see section 4.1). Most probably, a period of about 60-  
529 70 years is too short for pine forests to recover totally after being decimated by very cold  
530 conditions (cf. Kullman, 1986, 2005). We think that the distinct pine oscillation reflects a  
531 multi-decadal cold period whereby pine survived, but experienced reduced pollen production.  
532 According to Dahl et al. (2002), the 9.7 glacial advance at Jostedalsgreen, ca. 150 km WSW  
533 of Finnsjøen reflects a cooling of at least 1°C. This would have reduced the pine pollen  
534 production by a similar magnitude as displayed in the Finnsjøen pollen diagram (cf. Hicks,  
535 2006).

536

537 Notably, at Flåfattjønnna, an erosion layer distinctly reflects the 9.7 event. This layer including  
538 pine seeds and needles shows that pine pollen percentages and LOI decrease after the decline  
539 in pine PAR (Paus, 2010). The pine percentage maximum at the pine PAR minimum (Fig. 4)  
540 reflects outwash of soils containing remains of local pine (pollen and macrofossils) when  
541 regional and local total pollen production was reduced (Paus, 2010). In addition, at  
542 Flåfattjønnna, PCA indicates regression of local vegetation towards pioneer stages during the  
543 9.7 event (Fig. 9).

544  
545 According to the radiocarbon chronology (Fig. 3a), this cold event occurred ca. 9605-9675 cal  
546 yrs. BP interpolated (Figs. 2), but the varves suggest the duration to be around 56-58 years  
547 (Fig. 7). At Flåfattjønnna, the cold event is predicted based on fewer  $^{14}\text{C}$  dates (Fig. 4). This  
548 low-resolution and inaccurate chronology dates the event to ca. 9500-9700 cal yrs. BP (Paus,  
549 2010).

550

### 551 5.5. The 9.3 cold event

552 At both Flåfattjønnna and Finnsjøen, the post-9.7 warming initiated a vegetation closure  
553 reaching the Holocene maximum according to total PAR (Fig. 4). At Finnsjøen, the  
554 vegetation closure strongly reduced palynological richness. This warming also initiated the  
555 rapid establishment of broad pine-forest belts in mid-Scandinavia, reflecting the July mean  
556 Holocene maximum (Paus and Haugland, 2017). Shortly thereafter, during the first half in  
557 Finnsjøen PAZ S-4 (Fig. 6), a small-scale cooling parallel to the 9.7 event is detected around  
558 9300 cal yrs. BP (at 1963 cm depth, see also table 2), showing a minimum in sediment density  
559 and decreasing pine, and a delayed increase in freshwater algae (*Pediastrum*, *Botryococcus*;  
560 Figs. 2, 6). Furthermore, local vegetation became more open shown by decreasing total PAR  
561 (Fig. 5), increasing light-demanding shrubs and dwarf-shrubs (Fig. 6), and an increase in  
562 long-distance pollen (cf. *Corylus*). We think these changes reflect a climate cooling, though

563 its local effect was less extensive than the 9.7 impact at Finnsjøen. As for the 9.7 event, the  
564 delayed increase in freshwater algae could indicate the warming following the short-lasting  
565 cold event. The 9.3 cooling reflects the collapse of the Laurentide Ice Sheet (Yu et al., 2010;  
566 Gavin et al., 2011) with distinct impacts in Canada (Gavin et al., 2011), Greenland (Young et  
567 al. 2013), Iceland (Brynjolfson et al., 2015), and further south at the Iberian Peninsula  
568 (Burjachs et al., 2016; Iriarte-Chiapusso et al., 2016). The 9.3 event is also recorded in the  
569 Greenland ice-cores (Vinther et al., 2009; Rasmussen et al., 2014). Furthermore, signals of  
570 the 9.3 south of Svalbard are weak (Werner et al., 2016). This, in line with the scarcity of  
571 Fennoscandian 9.3 records in eastern Europe and its limited impact at Finnsjøen, indicate that  
572 the 9.3 cooling had its main influence in western and southern coastal Europe.

573

574 In Finnsjøen, the 9.7 event (Erdalen 2) and 9.3 event are recorded as two distinct separate  
575 events. We therefore emphasize that the 9.7 event, which seems to have a Fennoscandian  
576 origin, i.e. the drainage of the Baltic Ancylus Lake (Nesje et al., 2004), is not formally a  
577 “Bond” event, and must therefore not be confused with the 10.3 or 9.3 “Bond” events of  
578 North Atlantic Ocean origin (Bond et al., 1997, 2001).

579

#### 580 *5.6. The 8.2 cold event – Finse event*

581 At Finnsjøen, the post-9.3 changes with slight increase in vegetation density (Fig. 5), favored  
582 the moisture-demanding *Alnus* to expand within the area. Thereafter, stable records of  
583 vegetation and other parameters indicate a period of stable climate until ca. 8420 cal yrs. BP  
584 at the PAZ S-4/S-5 transition (Fig. 6), where colder temperatures are signaled. Here, pine  
585 percentages and PAR values decrease, probably due to a decline in summer temperatures that  
586 decreased regional pollen production (Paus and Haugland, 2017). The slightly later increase  
587 in tree-birch and alder PAR values (Fig. 5) could in addition reflect the lowering of vegetation  
588 belts within the region and the descent of the more warmth-demanding pine-forest. The rise in

589 *Alnus* PAR indicates the presence of more moist and fertile soils in the region, whereas  
590 macrofossils (Table 3) show the local presence of birch-forests. The increase in juniper (Figs.  
591 5 and 6) reflects more open vegetation locally, and PCA (Fig. 9) shows the recurrence  
592 towards more pioneer vegetation. The decreasing LOI and sediment density in the last part of  
593 S-5 (Fig. 2) point to increased soil erosion and outwash.

594  
595 Around the S-5/S-6 transition at ca. 8225 cal yrs. BP, pollen data indicate harsher conditions  
596 showing a maximum in palynological richness (Fig. 4) and representation of pioneers  
597 (*Saxifraga oppositifolia* type, *Empetrum*) in a short period with low total PAR between the  
598 earlier birch and alder decrease and the later pine rise in the pollen diagrams (Figs. 5 and 6).  
599 Apparently, the birch-forest ecotone was lowered which displaced the local area towards the  
600 tundra vegetation zone. This opening of local vegetation occurs at the same time when  
601 erosion of terrestrial organic matter intensified, and further supported by the short-lasting  
602 maximum in C/N-ratio (Fig. 2). Thereafter, the deposition of a dark minerogenic layer (Figs.  
603 2 and 7, Table 2) is initiated showing minimum sediment density, K, Ca, and LOI. This  
604 reflects maximum erosion and outwash due to deteriorating climate conditions. At the same  
605 time, an increase in pine in early S-6 (Figs. 5 and 6) reflects expanding regional pine-forests  
606 and/or increasing pine-pollen production. Both alternatives reflect warmer conditions during  
607 summer. A warmer lake could also be indicated by decreasing C/N values due to increased  
608 algal growth. This apparently contrasting evidence of climate points to the 8.2 weakening of  
609 the Atlantic current (Daley et al., 2011; Holmes et al., 2016) that resulted in an increased  
610 continental climate and enhanced amplitude of seasonal temperatures and involved at least  
611 colder winters (Alley and Ágústsdóttir, 2005). Hence, even if widespread local areas were  
612 exposed to maximum freezing/thawing and erosion due to a period of less snow and more  
613 wind during colder winters, summers became warm enough to allow regional pine to expand  
614 and/or increase its pollen production.



615

616 The bio- and litho-stratigraphy in PAZ S-5 and S-6 shows a two-step climate deterioration.  
617 The first of moderate impact is mainly signaled by the biostratigraphy at the PAZ S-4/S-5  
618 transition, from ca. 8420 cal yrs. BP, whereas the second and strongest period is mainly  
619 reflected by geochemistry and a dark erosional layer that deposited from ca. 8225 cal yrs. BP  
620 close to the PAZ S-5/S-6 transition. The varve chronology suggests that this dark layer spans  
621 a period of ca. 38 years (Fig. 7). Probably, missing sediments could add maximum 20 years to  
622 this duration (see section 4.1.), which indicates that climate deterioration intensified ca. 8245  
623 cal yrs. BP or a few years later. This coincides approximately with minimum  $\delta^{18}\text{O}$ -derived  
624 temperatures in the Greenland ice core (Fig. 2).

625

626 According to Rasmussen et al. (2014), the 8.2 event started ca. 8250 cal yrs. BP which is  
627 close to the estimated age of PAZ S-5/S-6 transition and the deposition of the erosion layer. It  
628 is likely these abrupt stratigraphical changes signal the sudden outburst of Lake Agassiz and  
629 the strong meltwater pulse into the North Atlantic that caused colder, drier and windier  
630 conditions globally (Alley et al., 1997; Alley and Áugústsdóttir, 2005). Most probably, the  
631 moderate changes ca. 8420 cal yrs. BP reflects a longer-term cooling upon which the 8.2  
632 event is superimposed (Rohling and Pälike, 2005).

633

634 A third phase, representing a recovery phase, from ca. 8175 to 8050 cal yrs. BP, shows  
635 increasing sediment density, K content, LOI, and total PAR (Figs. 2 and 5), which reflects  
636 stabilizing soils and re-development of vegetation cover. This long-lasting re-establishment  
637 phase of more than hundred years indicates that conditions gradually improved. The exposed  
638 position of Finnsjøen could partly explain the slow regrowth locally. On the other hand, the  
639 short-lasting algal-maximum ca. 8100 cal yrs. BP could indicate further warming that  
640 differentiates an older and still rather cold and unfavorable phase from a younger and warmer

641 phase. In total, 370 years elapsed extending from ca. 8420 to 8050 cal yrs. BP, before the  
642 Finnsjøen vegetation totally recovered from the 8.2 impact.

643

644 At Flåfattjønnna, the low-resolution chronology displays a 400 years local response (ca. 8550  
645 to 8150 cal yrs. BP; Paus, 2010) to the 8.2 (*sensu lato*) impact appearing in a two-step moist-  
646 dry pattern. However, both steps were regarded as cold periods (Paus, 2010). Similar two-step  
647 patterns are a wide-spread phenomenon as reported by other researchers (e.g. Nesje and Dahl,  
648 2001; Ojala et al., 2008; Rasmussen et al., 2008; Filoc et al. 2017). According to Rasmussen  
649 et al. (2014), the impact of the freshwater impulse into the North Atlantic lasted ca. 150 years  
650 (ca 8250 to 8090 cal yrs. BP), but terrestrial sites show longer-lasting responses of varying  
651 lengths (Filoc et al., 2017). Although a varying degree of dating precision must be considered,  
652 one must expect that the duration of vegetation responses to the same impact depends on both  
653 the geographical position (e.g. N-S, E-W, distance from coast) and distance from ecotones.  
654 Study sites at ecotonal positions, i.e. being less resilient to disturbance (such as the Finnsjøen  
655 and Flåfattjønnna sites), seem to show long-lasting responses to the 8.2 event. Such sites  
656 probably were more vulnerable to the background climate variations such as the 8.2 precursor  
657 (Rohling and Pälike, 2005). Most probably, ecotonal sites also show a slow recovery after  
658 cold events.

659

### 660 *5.7. The 9.7 and 8.2 events compared*

661 Both at Flåfattjønnna and Finnsjøen, the impact of the 8.2 event *sensu lato* (ca 370-400 years)  
662 lasted longer than the influence from the 9.7 cooling event (60 to < 200 years). At  
663 Flåfattjønnna, the distinct PCA responses (Figs. 4 and 9a) show that the 8.2 event had a  
664 stronger impact on local vegetation than the 9.7 event. At Finnsjøen, with a better  
665 stratigraphic time resolution than Flåfattjønnna, the strength of the two events could be  
666 reflected by increased sedimentation rate of their erosional layers. According to the varve

667 chronology, the sedimentation rate of the 9.7 erosional layer is ~ 4.4 cm during 56-58 years  
668 (0.79-0.76 mm/yr), whereas the 8.2 erosional layer show a sedimentation rate of ~2.8 cm  
669 during 38 years (0.74 mm/yr). On the other hand, the 8.2 erosion occurred at a higher  
670 successional stage with denser vegetation on more mature soils (Fig. 9), i.e. when local  
671 vegetation was at a distance from ecotones and more resilient to disturbance. In spite of that,  
672 erosion during the 8.2 event shows similar values as during the 9.7 cold spell. Hence, the 8.2  
673 cold event appears to have been stronger than the 9.7 cold event in the Finnsjøen area, and  
674 probably also over larger regions as signals of the 9.7 event are scarce.

675

676 To estimate patterns of impact, it would have been of interest to compare these results with  
677 studies from a wider area. To the best of our knowledge, other pollen records of the 9.7 event  
678 in Scandinavia are absent, whereas pollen signals of the 8.2 event are sparse in alpine south  
679 Norway.

680

681 At Topptjøna, 1.7 km south of Finnsjøen, the 8.2 event also shows a moist-dry two-step  
682 pattern, but the study was carried out with a much lower time resolution than at Finnsjøen  
683 (Paus et al., 2011). In Jotunheimen, ca. 110 km SW of Finnsjøen, the 8.2 event appears as a  
684 short reduction in pine pollen (Barnett et al. 2001; Gunnarsdottir, 1996). The Leirdalen site of  
685 Barnett et al. (2001) shows a strong pine oscillation from 90 % to 45 % and back to 90 %,  
686 lasting less than 80 years. Pine stomata show the presence of pine during the pine pollen  
687 minimum. Otherwise, the pollen percentages of *Betula*, *Salix* and herbs increased. This has  
688 been interpreted as a short-lasting cold event that affected pine pollen production but not the  
689 vegetative growth locally (Hicks, 2006). The similar pollen-stratigraphical patterns during the  
690 short-lasting Finnsjøen 9.7 event have been interpreted similarly (see section 5.4). During the  
691 9.7 event, Finnsjøen was lying in open birch-forests well above the pine-forest line (see  
692 section 5.2.), whereas the Leirdalen site (920 m a.s.l.) was situated in closed pine-forests

693 during the 8.2 event and far below the upper pine-forest ecotone. Even being situated at  
694 opposite sides of an ecotone, the border between pine-forest and birch-forest, the two sites  
695 showed similar pollen responses to the weaker 9.7 and the stronger 8.2 cooling, respectively.  
696 This demonstrates how vegetation response is determined by both the impact and the ecotonal  
697 position of the vegetation cover (cf. Smith, 1965; Fægri and Iversen, 1989)

698

## 699 **6. Conclusions**

700

- 701 • The sediments of Finnsjøen and Flåfattjønnna show exceptionally strong stratigraphical  
702 signals of the 9.7 and 8.2 cooling events. The positions of these sites close to ecotones  
703 (vegetation borders) were decisive in reducing their resilience against climate  
704 fluctuations.
- 705 • At Finnsjøen and Flåfattjønnna, the impact of the 8.2 event was stronger than the 9.7  
706 event.
- 707 • During the abrupt 9.7 cooling event at Finnsjøen, pine pollen percentages became  
708 halved and re-established in less than 60 years indicating that pine pollen production  
709 was severely reduced due to lower summer temperatures.
- 710 • At Finnsjøen, the 8.2 event *sensu lato* (ca. 8420 – 8050 cal yrs. BP) can be divided  
711 into a precursor lasting ca. 195 years, an erosional phase lasting ca. 50 years, and a  
712 recovery phase lasting ca. 125 years. At the onset of the erosional phase, summer  
713 temperatures increased.
- 714 • In the Finnsjøen sediments, weak signals indicate a cold spell at 9300 cal yrs. BP.  
715 Both the 8.2 and 9.3 events reflect collapses of the Laurentide Ice Sheet and represent  
716 two of the global “Bond” events. The 9.7 event most probably reflects the drainage of  
717 the Baltic Ancylus Lake that had restricted regional impact.

- 718 • The XRF sediment density graph documents annual varves throughout the studied  
719 Finnsjøen sediments.
- 720 • br-GDGT-based temperatures are biased towards warmer seasons and indicate gradual  
721 cooling throughout the Early Holocene, following local summer insolation.
- 722 • C/N ratios indicate input of lacustrine algal production and higher plant matter from  
723 the catchment area.
- 724 • Higher C/N values coincide with the onset of cold events and declines with its  
725 intensification; C/N increases again after the cold period.
- 726 • Input of terrestrial organic matter (plant waxes) decreases during cold conditions  
727 followed by its steady increase afterwards.

728

729

### 730 **Acknowledgements**

731 We thank Espen Paus, Erling Straalberg, and Ståle Samuelshaug for help during coring. The  
732 ITRAX  $\mu$ XRF core scanner system at the EARTHLAB, Department of Earth Science,  
733 University of Bergen, was used for elemental analyses, color and x-ray image scanning of the  
734 core. We also want to thank two anonymous reviewers for valuable comments which  
735 significantly improved the manuscript.

736

### 737 **Funding sources**

738 This work was financially supported by the Olaf Grolle-Olsen and Meltzer University  
739 Foundations

740

### 741 **References**

742 Aario, L., 1940. Waldgrenzen und subrezente Pollenspektern in Petsamo Lappland. *Annales*

743 *Academia Scientiarum Fennica A* 54 (8), 1-120.

744 Alley, R.B., Mayewski, P.A., Sowers, T., Stuiver, M., Taylor, K.C. and Clark, P.U., 1997.  
745 Holocene climatic instability: A prominent, widespread event 8200 yr ago. *Geology*  
746 25(6), 483–486.

747 Alley, B., Ágústsdóttir, A.M., 2005. The 8k event: cause and consequences of a major  
748 Holocene abrupt climate change. *Quaternary Science Reviews* 24, 1123-1149,  
749 doi:10.1016/j.quascirev.2004.12.004.

750 Andersen, C., Koc, N., Moros, M., 2004. A highly unstable Holocene climate in the subpolar  
751 North Atlantic: evidence from diatoms *Quaternary Science Reviews* 23, 2155-2166.  
752 doi:10.1016/j.quascirev.2004.08.004.

753 Bakke, J., Dahl, S.O., Nesje, A., 2005. Lateglacial and early Holocene palaeoclimatic  
754 reconstruction based on glacier fluctuations and equilibrium-line altitudes at northern  
755 Folgefonna, Hardanger, western Norway. *Journal of Quaternary Science* 20, 279–  
756 298, doi:10.1002/jqs.893.

757 Bergman, J., Hammarlund, D., Hannon, G., Barnekow, L., Wohlfarth, B., 2005. Deglacial  
758 vegetation succession and Holocene tree-limit dynamics in the Scandes Mountains,  
759 west-central Sweden: stratigraphic data compared to megafossil evidence. *Review of*  
760 *Palaeobotany and Palynology* 134, 129-151, doi:10.1016/j.revpalbo.2004.12.005.

761 Barnett, C., Dumayne-Peaty, L., Matthews, J.A., 2001. Holocene climatic change and tree-  
762 line response in Leirdalen, central Jotunheimen, south central Norway. *Review of*  
763 *Palaeobotany and Palynology* 117, 119-137.

764 Berger, A.L., 1978. Long term variations of daily insolation and Quaternary climate change.  
765 *Journal of Atmospheric Science* 35, 2362-2367.

766 Berner, K.S., Koç, N., Divine, D., Godtliabsen, F., 2008. Decadal-scale Holocene sea surface  
767 temperature record from the sub-polar North Atlantic: evaluating the effects of Bonds

768 icrafting episodes on the regional SSTs. *Paleoceanography* 23, PA2210,  
769 doi:10.1029/2006PA001339.

770 Berner, K.S., Koç, N., Godtlielsen, F., 2010, High frequency climate variability of the  
771 Norwegian Atlantic Current during the early Holocene period and a possible  
772 connection to the Gleissberg cycle. *The Holocene* 20(2), 245–255,  
773 doi:10.1177/0959683609350391.

774 Birks, H.J.B., Line, J.M.L., 1992. The use of rarefaction analysis for estimating palynological  
775 richness from Quaternary pollen-analytical data. *The Holocene* 2, 1-10.

776 Björck, S., Rundgren, M., Ingólfsson, Ó., Funder, S., 1997. The Preboreal oscillation around  
777 the Nordic Seas: terrestrial and lacustrine responses. *Journal of Quaternary Science*  
778 12, 455-465.

779 Bjune, A.E., 2005. Holocene vegetation history and tree-line changes on a north-south  
780 transect crossing major climate gradients in southern Norway – evidence from pollen  
781 and plant macrofossils in lake sediments. *Review of Palaeobotany and Palynology*  
782 133, 49–275, doi:10.1016/j.revpalbo.2004.10.005.

783 Blaauw, M., 2010. Methods and code for 'classical' age-modelling of radiocarbon  
784 sequences. *Quaternary Geochronology* 5, 512-518, doi:10.1016/j.quageo.2010.01.002.

785  
786 Bond, G., Showers, W., Cheseby, M., Lotti, R., Almasi, P., de Menocal, P., Priore, P., Cullen,  
787 H., Hajdas, I., Bonani, G., 1997. A pervasive millennial-scale cycle in the North  
788 Atlantic Holocene and glacial climates. *Science* 294, 2130-2136.

789 Bond, G., Kromer, B., Beer, J., Muscheler, R., Evans, M.N., Showers, W., Hoffmann, S.,  
790 Lotti-Bond, R., Hajdas, I., Bonani, G., 2001. Persistent solar influence on North  
791 Atlantic climate during the Holocene. *Science* 278, 1257-1266,  
792 doi:10.1126/science.1065680.

793 Bos, J.A.A., van Geel, B, van der Plicht, J, Bohncke, S., 2007. Preboreal climate oscillations  
794 in Europe: Wiggle-match dating and synthesis of Dutch high-resolution multi-proxy  
795 records. *Quaternary Science Reviews* 26, 1927–1950,  
796 doi:10.1016/j.quascirev.2006.09.012.

797 Brynjolfsson, S., Schomacker, A., Ingolfsson, O., Keiding, J.K., 2105. Cosmogenic <sup>36</sup>Cl  
798 exposure ages reveal a 9.3 ka BP glacier advance and the Late Weichselian-Early  
799 Holocene glacial history of the Drangajökull region, northwest Iceland. *Quaternary*  
800 *Science Reviews* 126, 140-157, doi:10.1016/j.quascirev.2015.09.001.

801 Budja, M., 2007. The 8200 cal yrs. BP “climate event” and the process of neolithisation in  
802 south-east Europe. *Documenta Praehistorica* XXXIV, 191-201.

803 Burjachs, F., Jones, S.E., Giralt, S., Fernandez-Lopez de Pablo, J., 2016. Lateglacial to Early  
804 Holocene recursive aridity events in the SE Mediterranean Iberian Peninsula: The  
805 Salines playa lake case study. *Quaternary International* 403, 187-200,  
806 doi:10.1016/j.quaint.2015.10.117.

807 Dahl, S.O., Nesje, A., Lie, Ø., Fjordheim, K., Matthews, J.A., 2002. Timing, equilibrium-line  
808 altitudes and climatic implications of two early-Holocene glacier readvances during  
809 the Erdalen Event at Jostedalsbreen, western Norway. *The Holocene* 12, 17–25,  
810 doi:10.1191/0959683602hl516rp.

811 Daley, T.J., Thomas, E.R., Holmes, J.A., Street-Perrott, F.A., Chapman, M.R., Tindall, J.C.,  
812 Valdes, P.J., Loader, N.J., Marshall, J.D., Wolff, E.W., Hopley, P.J., Atkinson, T.,  
813 Barber, K.E., Fisher, E.H., Robertson, I., Hughes, P.D.M., Roberts, C.N., 2011. The  
814 8200 yr BP cold event in stable isotope records from the north Atlantic region. *Global*  
815 *and Planetary Change* 79, 288-302, doi:10.1016/j.gloplacha.2011.03.006.

816 Das, S.K., Routh, J., Roychoudhury, A.N., Val Klump, J., 2008. Elemental (C, N, H and P)  
817 and stable isotope ( $\delta^{15}\text{N}$  and  $\delta^{13}\text{C}$ ) signatures in sediments from Zeekoevlei, South



818 Africa: a record of human intervention in the lake. *Journal of Paleolimnology* 39, 349-  
819 360, doi:10.1007/s10933-007-9110-5.

820 Davis, M.B., Moeller, R.E, Brubaker, L.B., 1984. Sediment focusing and pollen influx. In:  
821 Haworth, E.Y, Lund, J.W.G. (eds.): *Lake sediments and environmental history*, 261-293.  
822 University of Leicester, Leicester.

823 Davis, B.A.S., Stevenson, A.C., 2007. The 8.2 ka event and Early–Mid Holocene forests, fires  
824 and flooding in the Central Ebro Desert, NE Spain. *Quaternary Science Reviews* 26,  
825 1695-1712, doi:10.1016/j.quascirev.2007.04.007.

826 De Jonge, C., Hopmans, E.C., Stadnitskaia, A., Rijpstra, W.I.C., Hofland, R., Tegelaar, E.,  
827 Sinninghe Damsté, J.S., 2013. Identification of novel penta- and hexamethylated  
828 branched glycerol dialkyl glycerol tetraethers in peat using HPLC–MS<sup>2</sup>, GC–MS and  
829 GC–SMB-MS. *Organic Geochemistry* 54, 78-82,  
830 doi:10.1016/j.orggeochem.2012.10.004.

831 De Jonge, C., Hopmans, E.C., Zell, C.I., Kim, J.-H., Schouten, S., Sinninghe Damsté, J.S.,  
832 2014. Occurrence and abundance of 6-methyl branched glycerol dialkyl glycerol  
833 tetraethers in soils: implications for palaeoclimate reconstruction. *Geochimica et*  
834 *Cosmochimica Acta* 141, 97-112, doi: 10.1016/j.gca2014.06.013.

835 De Rosa, M., Gambacorta, A., 1988. The lipids of archaebacteria. *Progress in Lipid Research*  
836 27, 153-175, doi: 10.1016/0163-7827(88)90011-2.

837 Deng, L., Jia, G., Jin, C., Li, S., 2016. Warm season bias of branched GDGT temperature  
838 estimates causes underestimation of altitudinal lapse rate. *Organic Geochemistry* 96,  
839 11-17, doi: 10.1016/j.orggeochem.2016.03.004.

840 DNMI, 2016. The Norwegian meteorological Institute,  
841 [http://sharki.oslo.dnmi.no/portal/page?\\_pageid=73,39035,73\\_39049&\\_dad=portal&\\_s](http://sharki.oslo.dnmi.no/portal/page?_pageid=73,39035,73_39049&_dad=portal&_schema=PORTAL)  
842 [chema=PORTAL](http://sharki.oslo.dnmi.no/portal/page?_pageid=73,39035,73_39049&_dad=portal&_schema=PORTAL). Accessed April 2018.

843 Dormoy, I., Peyron, O., Combourieu Nebout, N., Goring, S., Kotthoff, U., Magny, M., Pross,  
844 J., 2009. Terrestrial climate variability and seasonality changes in the Mediterranean  
845 region between 15 000 and 4000 years BP deduced from marine pollen records.  
846 *Climate of the Past* 5, 615-632, doi:10.5194/cp-5-615-2009.

847 Ertl, C., Pessi, A.-M., Huusko, A., Hicks, S., Kubin, E., Heino, S., 2012. Assessing the  
848 proportion of “extra-local” pollen by means of modern aerobiological and  
849 phenological records — An example from Scots pine (*Pinus sylvestris* L.) in northern  
850 Finland. *Review of Palaeobotany and Palynology* 185, 1-12,  
851 doi:10.1016/j.revpalbo.2012.07.014.

852 Fægri, K., Iversen, J., 1989. *Textbook of pollen analysis: 4th revised edition* by Fægri, K.  
853 Kaland PE, Krzywinski K. Wiley, Chichester

854 Ficken, K.J., Li, B., Swain, D.L., Eglinton, G., 2000. An n-alkane proxy for the sedimentary  
855 input of submerged/floating freshwater aquatic macrophytes. *Org. Geochem.* 31,  
856 745–749, doi: 10.1016/S0146-6380(00)00081-4.

857 Filoc, M., Kupryjanowicz, M., Szeroczyńska, K., Suchora, M., Rządziejewicz, M., 2017.  
858 Environmental changes related to the 8.2-ka event and other climate fluctuations  
859 during the middle Holocene: Evidence from two dystrophic lakes in NE Poland. *The*  
860 *Holocene* 27(10), 1550-1566, doi: 10.1177/0959683617702233.

861 Gajewski, K., 1995. Modern and Holocene pollen assemblages from some small arctic lakes on  
862 Somerset Island, NWT, Canada. *Quaternary Research* 44, 228-236.

863 Gavin, D.G., Henderson, A.C.G., Westover, K.S., Fritz, S.C., Walker, I.C., Leng, M.J., Hu,  
864 F.S., 2011. Abrupt Holocene climate change and potential response to solar forcing in  
865 western Canada. *Quaternary Science Reviews* 30, 1243-1255,  
866 doi:10.1016/j.quascirev.2011.03.003.

867 Ghilardi, B., O’Connell, M., 2013. Early Holocene vegetation and climate dynamics with  
868 particular reference to the 8.2 ka event: pollen and macrofossil evidence from a small

869 lake in western Ireland. *Vegetation History and Archaeobotany* 22, 99–114,  
870 doi:10.1007/s00334-012-0367-x.

871 Gjerde, M., Bakke, J., Vasskog, K., Nesje, A., Hormes, A., 2016. Holocene glacier variability  
872 and Neoglacial hydroclimate at Ålfotbreen, western Norway. *Quaternary Science*  
873 *Reviews* 133, 28-47, doi: 10.1016/j.quascirev.2015.12.004.

874 Grime, J.P., 1973: Competitive exclusion in herbaceous vegetation. *Nature* 242, 344-347.

875 Grytnes, J.A., 2003. Species richness patterns of vascular plants along seven altitudinal  
876 transects in Norway. *Ecography* 26, 291-300.

877 Gunnarsdottir, H., 1996. Holocene vegetation history and forest-limit fluctuations in  
878 Smådalen, eastern Jotunheimen, South Norway. *Paläoklimaforschung* 20, 233– 256.

879 Haflidason, H., Sejrup, H.P., Klitgaard Kristensen, D., Johnsen, S., 1995. Coupled response of  
880 the late glacial climatic shifts of northwest Europe reflected in Greenland ice cores:  
881 Evidence from the northern North Sea. *Geology* 23(12), 1059-1062.

882 Hicks, S., 2006. When no pollen does not mean no trees. *Vegetation History and*  
883 *Archaeobotany* 15, 253–261, doi:10.1007/s00334-006-0063-9.

884 Hjelle, K.L., Halvorsen, L.S., Prøsch-Danielsen, L., Sugita, S., Paus, A., Kaland, P.E., Mehl,  
885 I.K., Overland, A., Danielsen, R., Høeg, H.I., Midtbø, I., 2018. Long-term changes in  
886 regional vegetation cover along the west coast of southern Norway: The importance of  
887 human impact. *Journal of Vegetation Science*. 12 pp., doi: 10.1111/jvs.12626.

888 Holmes J.A., Tindall, J., Roberts, N., Marshall, W., Marshall, J.D., Bingham, A., Feeser, I.,  
889 O'Connell, M., Atkinson, T., Jourdan, A.-L., March, A., Fisher, E.H., 2016. Lake  
890 isotope records of the 8200-year cooling event in western Ireland: Comparison with  
891 model simulations. *Quaternary Science Reviews* 131, 341-349, doi:  
892 10.1016/j.quascirev.2015.06.027.

893 Hopmans, E.C., Weijers, J.W.H., Schefuß, E., Herfort, L., Sinninghe Damsté, J.S., Schouten,  
894 S., 2004. A novel proxy for terrestrial organic matter in sediments based on branched

895 and isoprenoid tetraether lipids. *Earth and Planetary Science Letters* 224, 107-116,  
896 doi: 10.1016/j.epsl.2004.05.012.

897 Hopmans, E.C., Schouten, S., Sinninghe Damsté, J.S., 2016. The effect of improved  
898 chromatography on GDGT-based palaeoproxies. *Organic Geochemistry* 93, 1-6, doi:  
899 10.1016/j.orggeochem.2015.12.006.

900 Jensen, C., Vorren, K.-D., Mørkved, B., 2007. Annual pollen accumulation rate (PAR) at the  
901 boreal and alpine forest-line of north-western Norway, with special emphasis on  
902 *Pinus sylvestris* and *Betula pubescens*. *Review of Palaeobotany and Palynology* 144,  
903 337–361, doi:10.1016/j.revpalbo.2006.08.006.

904 Iriarte-Chiapusso, M.J., Munoz Sobrino, C., Gomez-Orellana, L., Hernandez-Beloqui, B.,  
905 García-Moreiras, I., Fernandez Rodriguez, C., Heiri, O., Lotter, A.F., Ramil-Rego, P.,  
906 2016. Reviewing the Lateglacial-Holocene transition in NW Iberia: A  
907 palaeoecological approach based on the comparison between dissimilar regions.  
908 *Quaternary International* 403, 211-236, doi: 10.1016/j.quaint.2015.09.029.

909 Kaland, P.E., Natvig, Ø. 1993. CORE 2.0., a computer program for stratigraphical data,  
910 developed at University of Bergen, Norway. Unpublished

911 Kullman, L., 1986. Late Holocene reproductional patterns of *Pinus sylvestris* and *Picea*  
912 *abies* at the forest limit in central Sweden. *Canadian Journal of Botany* 64, 1682–  
913 1690, doi:10.1139/b86-225.

914 Kullman, L., 2005. Pine (*Pinus sylvestris*) treeline study dynamics during the past millennium  
915 – a population study in west-central Sweden. *Annales Botanici Fennici* 42, 95-106.

916 Kullman, L., 2013. Ecological tree line history and palaeoclimate - review of megafossil  
917 evidence from the Swedish Scandes. *Boreas* 42, 555-567, doi:10.1111/bor.12003.

918 Loomis, S.E., Russell, J.M., Ladd, B., Street-Perrott, F.A., Sinninghe Damsté, J.S., 2012.  
919 Calibration and application of the branched GDGT temperature proxy on East African

920 lake sediments. *Earth and Planetary Science Letters* 357–358, 277–288, doi:  
921 10.1016/j.epsl.2012.09.031.

922 Moran, A.P., Kerschner, H., Ochs, S.I., 2016. Redating the moraines in the Kromer Valley  
923 (Silvretta Mountains) – New evidence for an early Holocene glacier advance. *The*  
924 *Holocene* 26(4), 655–664, doi: 10.1177/0959683615612571

925 Moore, P.D., Webb, J.A., Collinson, M.E., 1991. *Pollen analysis*. Blackwell Scientific  
926 Publications, Oxford.

927 Naafs, B.D.A., Inglis, G.N., Zheng, Y., Amesbury, M.J., Biester, H., Bindler, R., Blewett, J.,  
928 Burrows, M.A., del Castillo Torres, D., Chambers, F.M., Cohen, A.D., Evershed, R.P.,  
929 Feakins, S.J., Galka, M., Gallego-Sala, A., Gandois, L., Gray, D.M., Hatcher, P.G.,  
930 Honorio Coronado, E.N., Hughes, P.D.M., Huguet, A., Könönen, M., Laggoun-  
931 Défarge, F., Lähteenoja, O., Lamentowicz, M., Marchant, R., McClymont, E.,  
932 Pontevedra-Pombal, X., Ponton, C., Pourmand, A., Rizzuti, A.M., Rochefort, L.,  
933 Schellekens, J., De Vleeschouwer, F., Pancost, R.D., 2017. Introducing global peat-  
934 specific temperature and pH calibrations based on br-GDGT bacterial lipids.  
935 *Geochimica et Cosmochimica Acta* 208, 285–301, doi: 10.1016/j.gca.2017.01.038

936 Nesje, A., 1992. A piston corer for lacustrine and marine sediments. *Arctic Alpine Research* 24,  
937 257–259.

938 Nesje, A., Dahl, S.O., 2001. The Greenland 8200 cal. yr BP event detected in loss-on-ignition  
939 profiles in Norwegian lacustrine sediment sequences. *Journal of Quaternary Science*  
940 16, 155–166.

941 Nesje, A., Kvamme, M., Rye, N., Løvlie, R. 1991. Holocene glacial and climate history of the  
942 Jostedalbreen region, western Norway; evidence from lake sediments and terrestrial  
943 deposits. *Quaternary Science Reviews* 10, 87–114.

944 Nesje, A., Matthews, J.A., Dahl, S.O., Berrisford, M.S., Andersson, C., 2001. Holocene  
945 glacier fluctuations of Flatebreen and winter-precipitation changes in the

946 Jostedalbreen region, western Norway, based on glaciolacustrine sediment records.  
947 *The Holocene* 11, 267–280.

948 Nesje, A., Dahl, S.O., Bakke, J., 2004. Were abrupt Lateglacial and early-Holocene climatic  
949 changes in northwest Europe linked to freshwater outbursts to the North Atlantic and  
950 Arctic Oceans? *The Holocene* 14(2), 299–310. doi:10.1191/0959683604hl708fa

951 Nicolussi, K., Schlüchter, C., 2012. The 8.2 ka event—Calendar-dated glacier response in the  
952 Alps. *Geology* 40(9), 819-822, doi:10.1130/G32406.1

953 Obrochta, S.P., Miyahara, H., Yokoyama, Y., Crowley, T.J., 2012. A re-examination of  
954 evidence for the North Atlantic "1500-year cycle" at Site 609. *Quaternary Science*  
955 *Reviews* 55, 23-33, doi: 10.1016/j.quascirev.2012.08.008

956 Odland, A., 1996. Differences in the vertical distribution pattern of *Betula pubescens* in  
957 Norway and its ecological significance. *Paläoklimaforschung* 20, 43-59. Gustav  
958 Fischer Verlag, Stuttgart.

959 Ojala, A.K., Heinsalu, A., Kauppila, T., Alenius, T., Saarnisto, M., 2008. Characterizing  
960 changes in the sedimentary environment of a varved lake sediment record in southern  
961 central Finland around 8000 cal yr BP. *Journal of Quaternary Science* 23, 765–775,  
962 doi:10.1002/jqs.1157

963 Paus, A., 2010. Vegetation and environment of the Rødalen alpine area, Central Norway,  
964 with emphasis on the early Holocene. *Vegetation History and Archaeobotany* 19, 29-  
965 51, doi:10.1007/s00334-009-0228-4

966 Paus, A., 2013. Human impact, soil erosion, and vegetation response lags to climate change:  
967 Challenges for the mid-Scandinavian pollen-based transfer-function temperature  
968 reconstructions. *Vegetation History and Archaeobotany* 22(3), 269 – 284,  
969 doi:10.1007/s00334-012-0360-4

970 Paus, A., Haugland, V., 2017. Early- to mid-Holocene forest-line and climate dynamics in  
971 southern Scandes mountains inferred from contrasting megafossil and pollen data. *The*  
972 *Holocene* 27(3) 361–383, doi:10.1177/0959683616660172

973 Paus, A., Velle, G., Larsen, L., Nesje, A., Lie, Ø., 2006. Late-glacial nunataks in central  
974 Scandinavia: biostratigraphical evidence for ice thickness from Lake Flåfattjøna,  
975 Tynset, Norway. *Quaternary Science Reviews* 25, 1228-1246.

976 Paus, A., Velle, G., Berge, J., 2011. Late-glacial and early Holocene vegetation and  
977 environment in the Dovre mountains, central Norway, as signaled in two Late-glacial  
978 nunatak lakes. *Quaternary Science Reviews* 30, 1780-1793,  
979 doi:10.1016/j.quascirev.2005.10.008

980 Paus, A., Boessenkool, S., Brochmann, C., Epp, L.S., Fabel, D., Haflidason, H., Linge, H.,  
981 2015. Lake Store Finnsjøen - a key for understanding Late-Glacial/early Holocene  
982 vegetation and ice sheet dynamics in the central Scandes Mountains. *Quaternary*  
983 *Science Reviews* 121, 36-51, doi:10.1016/j.quascirev.2015.05.004

984 Peterse, F., Kim, J.-H., Schouten, S., Kristensen, D.K., Koç, N., Sinninghe Damsté, J.S.,  
985 2009. Constraints on the application of the MBT/CBT palaeothermometer at high  
986 latitude environments (Svalbard, Norway). *Organic Geochemistry* 40, 692-699, doi:  
987 10.1016/j.orggeochem.2009.03.004

988 Punt, W. et al., 1976-1996. *The Northwest European Pollen Flora* (NEPF) Vol I (1976), Vol II  
989 (1980), Vol III (1981), Vol IV (1984) Vol V (1988), Vol VI (1991), Vol VII (1996),  
990 Elsevier, Amsterdam.

991 Rasmussen, P., Hede, M.U., Noe-Nygaard, N., Clarke, A.L., Vinebrooke, R.D., 2008.  
992 Environmental response to the cold climate event 8200 years ago as recorded at Højby  
993 Sø, Denmark. *Geological Survey of Denmark and Greenland Bulletin* 15, 57-60.

994 Rasmussen, S.O., Bigler, M., Blockley, S.P., Blunier, T., Buchardt, S.L., Clausen, H.B.,  
995 Cvijanovic, I., Dahl-Jensen, D., Johnsen, S.J., Fischer, H., Gkinis, V., Guillevic, M.,

996 Hoek, W.Z., Lowe, J.J., Pedro, J.B., Popp, T., Seierstad, I.K., Steffensen, J.P.,  
997 Svensson, A.M., Vallelonga, P., Vinther, B.O., Walker, M.J.C., Wheatley, J.J.,  
998 Winstrup, M., 2014. A stratigraphic framework for abrupt climatic changes during the  
999 Last Glacial period based on three synchronized Greenland ice-core records: refining  
1000 and extending the INTIMATE event stratigraphy. *Quaternary Science Reviews* 106,  
1001 14-28, doi: 10.1016/j.quascirev.2014.09.007

1002 Reimer, P.J., Bard, E., Bayliss, A., Beck, J.W., Blackwell, P.G. et al., 2013. INTCAL13 and  
1003 MARINE13 radiocarbon age calibration curves 0-50,000 years cal yrs. BP.  
1004 *Radiocarbon* 55, 1869-1887.

1005 Renssen H, Goosse H, Fichetef T (2007) Simulation of Holocene cooling events in a coupled  
1006 climate model. *Quaternary Science Reviews* 26, 2019–2029,  
1007 doi:10.1016/j.quascirev.2007.07.011

1008 Rohling, E.J., Pälike, H., 2005. Centennial-scale climate cooling with a sudden cold event  
1009 around 8,200 years ago. *Nature* 43, 975–979, doi:10.1038/nature03421.

1010 Russell, J.M., Hopmans, E.C., Loomis, S.E., Liang, J., Sinninghe Damsté, J.S., 2018.  
1011 Distributions of 5- and 6-methyl branched glycerol dialkyl glycerol tetraethers (br-  
1012 GDGTs) in East African lake sediment: Effects of temperature, pH, and new lacustrine  
1013 paleotemperature calibrations. *Organic Geochemistry* 117, 56-69, doi:  
1014 10.1016/j.orggeochem.2017.12.003.

1015 Schouten, S., Hopmans, E.C., Pancost, R.D., Sinninghe Damsté, J.S., 2000. Widespread  
1016 occurrence of structurally diverse tetraether membrane lipids: Evidence for the  
1017 ubiquitous presence of low-temperature relatives of hyperthermophiles. *Proceedings*  
1018 *of the National Academy of Sciences* 97, 14421-14426, doi:  
1019 10.1073/pnas.97.26.14421.



- 1020 Schouten, S., Hopmans, E.C., Sinninghe Damsté, J.S., 2013. The organic geochemistry of  
1021 glycerol dialkyl glycerol tetraether lipids: A review. *Organic Geochemistry* 54, 19-61,  
1022 doi: 10.1016/j.orggeochem.2012.09.006.
- 1023 Seddon, A.W.R., Macias-Fauria, Willis., K.J., 2015. Climate and abrupt vegetation change in  
1024 Northern Europe since the last deglaciation. *The Holocene* 25(1), 25-36, doi:  
1025 10.1177/0959683614556383.
- 1026 Segerström, U., von Stedingk, H., 2003. Early Holocene spruce, *Picea abies* (L.) Karst., in  
1027 west central Sweden as revealed by pollen analysis. *The Holocene* 13, 897–906,  
1028 doi:10.1191/0959683603hl672rp.
- 1029 Selsing, L., 1998. Subfossils of Scots pine (*Pinus sylvestris* L.) from the mountain area of  
1030 South Norway as the basis for a long tree-ring chronology. *Norsk Geografisk*  
1031 *Tidsskrift* 52, 89-103.
- 1032 Seppä, H., 1998. Postglacial trends in palynological richness in the northern Fennoscandian  
1033 tree-line area and their ecological interpretation. *The Holocene* 8, 43-53.
- 1034 Seppä, H., Hicks, S., 2006. Integration of modern and past pollen accumulation rate (PAR)  
1035 records across the arctic tree-line: a method for more precise vegetation  
1036 reconstructions. *Quaternary Science Reviews* 25, 1501–1516,  
1037 doi:10.1016/j.quascirev.2005.12.002.
- 1038 Seppä, H., Birks, H. J. B., Giesecke, T., Hammarlund, D., Alenius, T., Antonsson, K., Bjune,  
1039 A.E., Heikkilä, M., MacDonald, G.M., Ojala, A.E.K., Telford, R.J., Veski, S., 2007.  
1040 Spatial structure of the 8200 cal yr BP event in northern Europe. *Climate of the Past* 3,  
1041 225-236.
- 1042 Simonsen, A., 1980. Vertical variations of Holocene pollen sedimentation at Ulvik, Hardanger,  
1043 SW-Norway (in Norwegian). *AmS-Varia* 8, 86 pp.

1044 Sinninghe Damsté, J.S., Hopmans, E.C., Pancost, R.D., Schouten, S., Geenevasen, J.A.J.,  
1045 2000. Newly discovered non-isoprenoid glycerol dialkyl glycerol tetraether lipids in  
1046 sediments. *Chemical Communications*, 1683-1684, doi:10.1039/B004517I.

1047 Sinninghe Damsté, J.S., Schouten, S., Hopmans, E.C., van Duin, A.C.T., Geenevasen, J.A.J.,  
1048 2002. Crenarchaeol: the characteristic core glycerol dibiphytanyl glycerol tetraether  
1049 membrane lipid of cosmopolitan pelagic crenarchaeota. *Journal of Lipid Research* 43,  
1050 1641-1651, doi:10.1194/jlr.M200148-JLR200.

1051 Smith AG (1965) Problems of inertia and thresholds related to post Glacial habitat changes.  
1052 *Proceedings of the Royal Society London B* 161, 331-342.

1053 Stockmarr, J., 1971. Tablets with spores in absolute pollen analysis. *Pollen Spores* 13, 615–  
1054 621.

1055 Stranne, C., Jakobsson, M., Björk, G., 2014. Arctic Ocean perennial sea ice breakdown during  
1056 the Early Holocene Insolation Maximum. *Quaternary Science Reviews* 92, 123-132,  
1057 doi:10.1016/j.quascirev.2013.10.022.

1058 Stuiver, M., Reimer, P.J., Reimer, R.W., 2018. CALIB 7.1 [WWW program] at  
1059 <http://calib.org>, accessed June 2018.

1060 Terasmaë, J., 1951. On the pollen morphology of *Betula nana*. *Svensk Botanisk Tidskrift* 45,  
1061 358–361.

1062 ter Braak, C.J.F., Smilauer, P., 1997- 2002. CANOCO for Windows, version 4.5 Biometrics –  
1063 Plant Research International, Wageningen, the Netherlands.

1064 Thoen, M.W., 2016. *Effekt og omfang av 9.7- og 8.2 kulde-eventene ved Store Finnsjøen på*  
1065 *Dovre fjell*. Master thesis, University of Bergen, Norway. 47 pp.  
1066 [https://bora.uib.no/bitstream/handle/1956/15529/152904321.pdf?sequence=1&isAllow](https://bora.uib.no/bitstream/handle/1956/15529/152904321.pdf?sequence=1&isAllowed=y)  
1067 [ed=y](https://bora.uib.no/bitstream/handle/1956/15529/152904321.pdf?sequence=1&isAllowed=y)  
1068

- 1069 Troels-Smith, J., 1955. Karakterisering av løse jordarter. *Danmarks Geologiske Undersøgelse*  
1070 IV. Række 3, 73 pp.
- 1071 van der Horn, S.A., van Kolfschoten T., van der Plicht, J., 2015. The effects of the 8.2 ka  
1072 event on the natural environment of Tell Sabi Abyad, Syria: Implications for  
1073 ecosystem resilience studies. *Quaternary International* 378, 111-118,  
1074 doi:10.1016/j.quaint.2015.04.005.
- 1075 Velle, G., Larsen, J., Eide, W., Peglar, S., Birks, H.J.B., 2005. Holocene environmental  
1076 history and climate of Råtåsjøen, a low-alpine lake in central Norway. *Journal of*  
1077 *Paleolimnology* 33, 129-153.
- 1078 Vinther, B. M., Buchardt, S.L., Clausen, H.B., Dahl-Jensen, D., Johnsen, S.J., Fisher, D.A.,  
1079 Koerner, R.M., Raynaud, D., Lipenkov, V., Andersen, K.K., Blunier, T., Rasmussen,  
1080 S.O., Steffensen, J.P., Svensson, A.M., 2009. Holocene thinning of the Greenland ice  
1081 sheet. *Nature* 461, 385-388, doi:10.1038/nature08355.
- 1082 Wanner, H., Solomina, O., Grosjean, M., Jetel, M., 2011. Structure and origin of Holocene  
1083 cold events. *Quaternary Science Reviews* 30, 3109-3123,  
1084 doi:10.1016/j.quascirev.2011.07.010.
- 1085 Weber, Y., De Jonge, C., Rijpstra, W.I.C., Hopmans, E.C., Stadnitskaia, A., Schubert, C.J.,  
1086 Lehmann, M.F., Sinninghe Damsté, J.S., Niemann, H., 2015. Identification and carbon  
1087 isotope composition of a novel branched GDGT isomer in lake sediments: Evidence  
1088 for lacustrine branched GDGT production. *Geochimica et Cosmochimica Acta* 154,  
1089 118-129, doi:10.1016/j.gca2015.01.032.
- 1090 Weijers, J.W.H., Schouten, S., van den Donker, J.C., Hopmans, E.C., Sinninghe Damsté, J.S.,  
1091 2007. Environmental controls on bacterial tetraether membrane lipid distribution in  
1092 soils. *Geochimica et Cosmochimica Acta* 71, 703-713, doi:10.1016/j.gca2006.10.003
- 1093 Weijers, J.W.H., Bernhardt, B., Peterse, F., Werne, J.P., Dungait, J.A.J., Schouten, S.,  
1094 Sinninghe Damsté, J.S., 2011. Absence of seasonal patterns in MBT–CBT indices in

1095 mid-latitude soils. *Geochimica et Cosmochimica Acta* 75, 3179-3190,  
1096 doi:10.1016/j.gca2011.03.015.

1097 Weijers, J.W.H., Bernhardt, B., Peterse, F., Werne, J.P., Dungait, J.A.J., Schouten, S.,  
1098 Sinninghe Damsté, J.S., 2011. Absence of seasonal patterns in MBT–CBT indices in  
1099 mid-latitude soils. *Geochimica et Cosmochimica Acta* 75, 3179-3190,  
1100 doi:10.1016/j.gca2011.03.015..

1101 Whittington, G., Edwards, K.J., Zanchetta, G., Keen, D.H., Bunting, M.J., Fallick, A.E.,  
1102 Bryant, C.L., 2015. Lateglacial and early Holocene climates of the Atlantic margins of  
1103 Europe: Stable isotope, mollusc and pollen records from Orkney, Scotland.  
1104 *Quaternary Science Reviews* 122, 112-130, doi:10.1016/j.quascirev.2015.05.026.

1105 Wohlfarth, B., Schwark, L., Bennike, O., Filimonova, L., Tarasov, P., Björkman, L.,  
1106 Brunnberg, L., Demidov, I., Possnert, G., 2004. Unstable early-Holocene climatic and  
1107 environmental conditions in northwestern Russia derived from a multidisciplinary  
1108 study of a lek-sediment sequence from Pichozero, southeastern Russian Karelia. *The*  
1109 *Holocene* 14(5), 732-746, doi:10.1191/0959683604hl751rp.

1110 Young, N.E., Briner, J.P., Rood, D.H., Finkel, R.C., Corbett, L.B., Bierman, P.R., 2013. Age  
1111 of the Fjord Stade moraines in the Disko Bugt region, western Greenland, and the 9.3  
1112 and 8.2 ka cooling events. *Quaternary Science Reviews* 60, 76-90,  
1113 doi:10.1016/j.quascirev.2012.09.028.

1114 Yu, S.H., Colman, S.M., Lowell, T.W., Milne, G.A., Fisher, T.G., Breckenridge, A., Boyd,  
1115 M., Teller, J.T., 2010. Freshwater Outburst from Lake Superior as a Trigger for the  
1116 Cold Event 9300 Years Ago. *Science* 328, 1262-1266, doi:10.1126/science.1187860.

1117 Zheng, Y., Zhou, W., Meyers, P.A., Xie, S., 2007. Lipid biomarkers in the Zoigê-Hongyuan  
1118 peat deposit: indicators of Holocene climate changes in West China. *Org. Geochem.*  
1119 38, 1927–1940, doi: 10.1016/j.orggeochem.2007.06.012.

1120 Zolitschka, B., Francus, P., Ojala, A.E.K., Schimmelmann, A. 2016. Varves in lake  
1121 sediments - a review. *Quaternary Science Reviews* 117, 1-41.

1122

1123

1124

1125

1126

### 1127 **Figure and table captions**

1128

1129 Fig. 1: Maps of the Lake Finnsjøen and Lake Flåfattjønnå areas. Numbers show altitudes in m  
1130 a.s.l.

1131 Fig. 2: Selected sediment features from the Finnsjøen core displayed along the linear  
1132 age/depth model. From left: X-ray colour image, pollen-assemblage zones (PAZ),  
1133 XRF scanning results of sediment density, K and Ca (cps: counts per second), loss-on-  
1134 ignition (LOI), *Pinus* and *Pediastrum* percentages, temperature deviations from  
1135 present in °C based on <sup>18</sup>O values from the Renland ice core, Greenland (Vinther et  
1136 al., 2009), C/N ratios, *n*-Alkanes (terrestrial organic matter and aquatic input), br-  
1137 GDGT-based estimates of pH and mean annual temperatures (MAT<sub>mr</sub>), and mid-  
1138 month summer solar insolation 60 °N (Berger, 1978). The 9.7, 9.3, and 8.2 cold events  
1139 are shaded. The 8.2 event (*sensu lato*) is displayed by a tripartite development: the  
1140 early precursor from ca. 8420 cal yrs. BP, the erosional phase from ca. 8225 cal yrs.  
1141 BP, and the recovery phase from ca. 8175 to ca. 8050 cal yrs. BP. Stippled red lines  
1142 show the one cm thick sediment slice missing from the core (see section 3.1).

1143

1144 Fig. 3: a): Age-depth relationship for the Finnsjøen sediments. Grey area illustrates the 95%  
1145 probability range. Two outliers marked with bold crosses, are recognized. The average

1146 linear sedimentation rate (white line) represents the preferred chronology (see section  
1147 3.3).

1148 b): The floating varve chronology based on microscale patterns of the XRF  
1149 sediment density graph and compared with the radiocarbon based age-depth  
1150 chronology. The youngest part of the varve chronology is tentatively attached to the  
1151 uppermost level 7600 cal yrs. BP dated by the radiocarbon-based age-depth model.

1152

1153 Fig. 4: Comparison of selected features from the Finnsjøen and Flåfattjønnna merged data set.

1154 The 9.7 and 8.2 cold events are shaded. Radiocarbon-dated levels are marked in the

1155 Flåfattjønnna age column. Shaded curves are 10x exaggerations of the scale.

1156

1157 Fig. 5: Pollen accumulation rates (PAR) for selected Finnsjøen taxa. Shaded curves are 10x

1158 exaggerations of the scale.

1159

1160 Fig. 6: Pollen percentage diagram from Finnsjøen. Calibrated dates are shown as mean

1161 probabilities (Stuiver et al., 2018). Shaded curves are 10x exaggerations of the scale.

1162

1163 Fig. 7: Detailed data of the 9.7 and 8.2 events at Finnsjøen. Figure displays scanning results

1164 (Xray colour image, sediment density, the elements K and Ca, loss-on-ignition (LOI),

1165 and temperature deviation (°C) from present based on  $^{18}\text{O}$  values in Renland ice core,

1166 Greenland (Vinther et al., 2009). To the right, the enlarged sediment densities during

1167 the 9.7 and 8.2 erosion layers show couplets of alternating maxima and minima values

1168 representing varves. Shading highlights the 9.7 and the 8.2 erosion layers.

1169

1170 Fig. 8: Plot of pollen taxa along the first two axes of the PCA of the merged pollen data set

1171 from Flåfattjønnna and Finnsjøen. Merged data set includes 121 samples, 108 terrestrial

1172 taxa. Eigenvalues axis 1: 0.5020, axis 2: 0.1578, axis 3: 0.0896, axis 4: 0.0502. In the  
1173 analysis, *Pinus* was treated as a passive taxon whereas loss-on-ignition (LOI) and  
1174 palynological richness (PR) were included as environmental variables. See section 5.3  
1175 for ecological interpretations of the axes.

1176

1177 Fig. 9: PCA of spectra from Flåfattjønna (a) and Finnsjøen (b). Pollen assemblage zones  
1178 (PAZ) follow Paus (2010) and Fig. 6. Levels in PAZ S-4 are not encircled. Figures  
1179 show the general vegetation development and the 9.7 and 8.2 impacts on vegetation in  
1180 a two-dimensional gradient space. See section 5.3 for ecological interpretations of the  
1181 axes. The data from the two lakes are from the same time interval: 7600 - 10.700 cal  
1182 yrs. BP.

1183

1184 Table 1: General features of the sites studied. Local temperatures are extrapolated from the  
1185 nearest meteorological stations (DNMI, 2016) using a lapse rate of 0.6 °C change per  
1186 100 m.

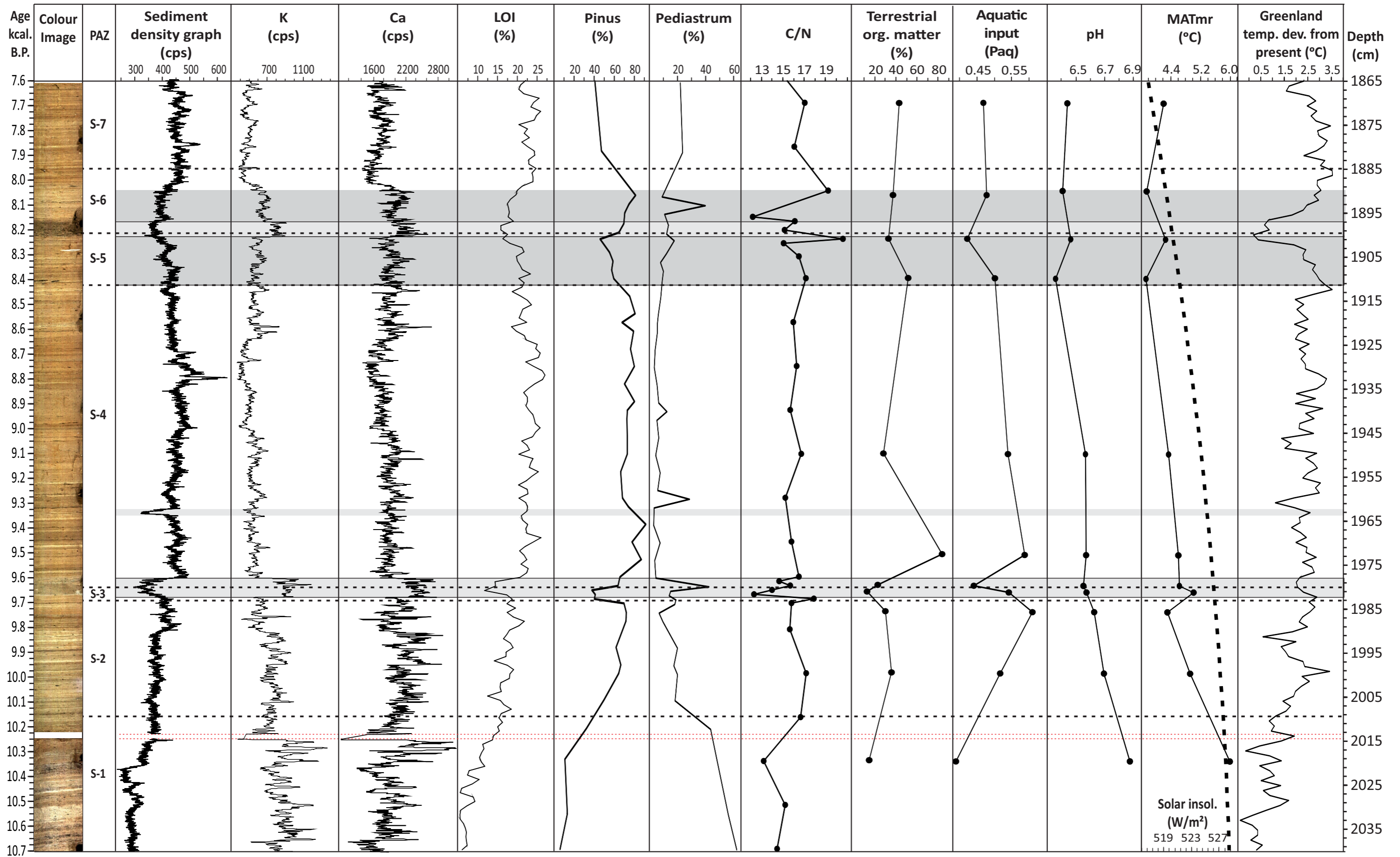
1187 Table 2: Description of the Finnsjøen sediment lithology.

1188

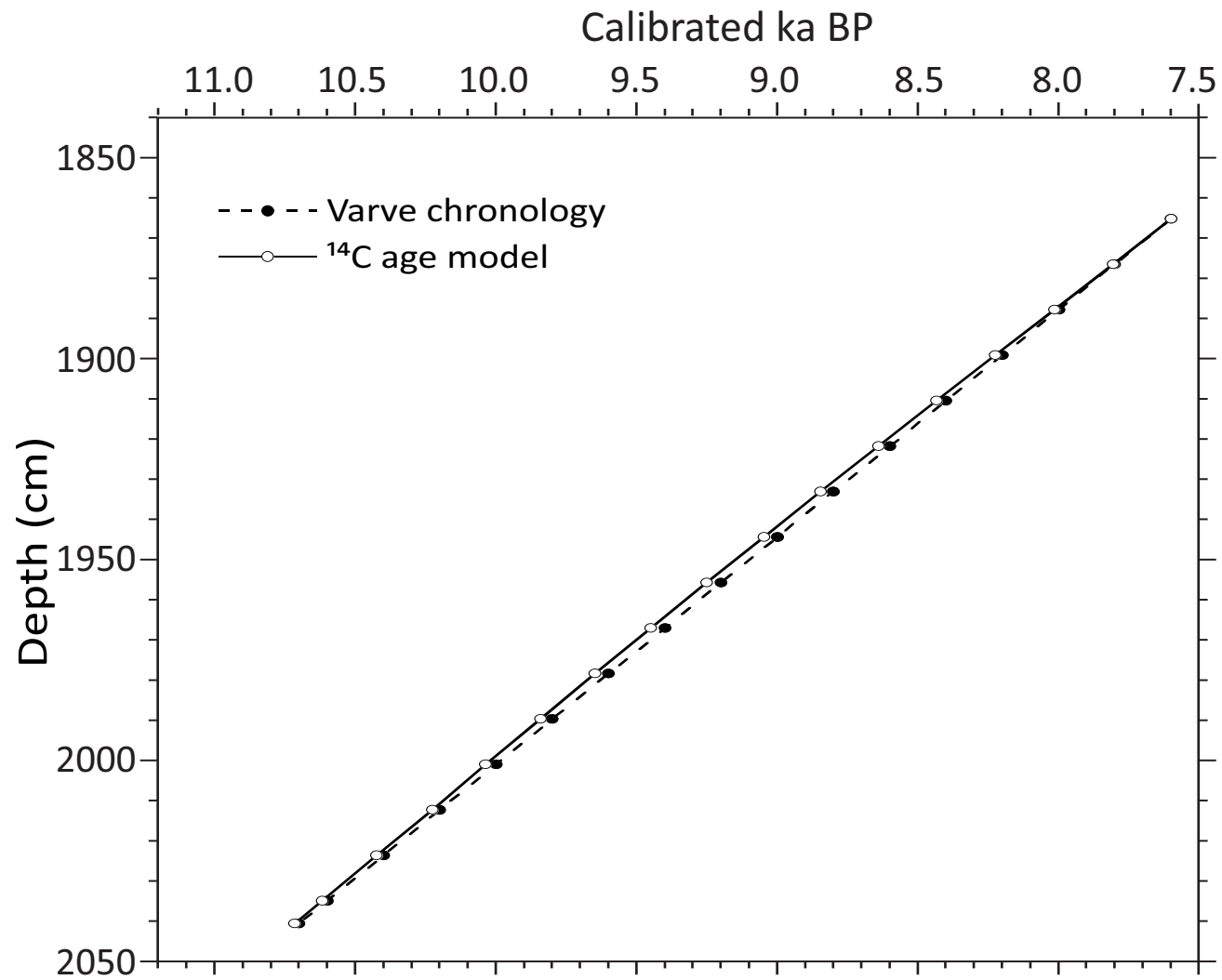
1189 Table 3: Results of seven AMS dates of plant macrofossils from Finnsjøen. Calibrated dates  
1190 according to Stuiver et al. (2018) are shown with two standard deviations. When  
1191 dating results appear as two or more intervals, the two extreme values define the  
1192 interval displayed. Median probabilities are shown in brackets. Lab. reference  
1193 numbers of two outliers are marked with <sup>A</sup>: ETH-48538 <sup>A</sup> and TRa-4470 <sup>A</sup>. Dates  
1194 previously published (Paus et al., 2015), are marked with an asterisk.

1195

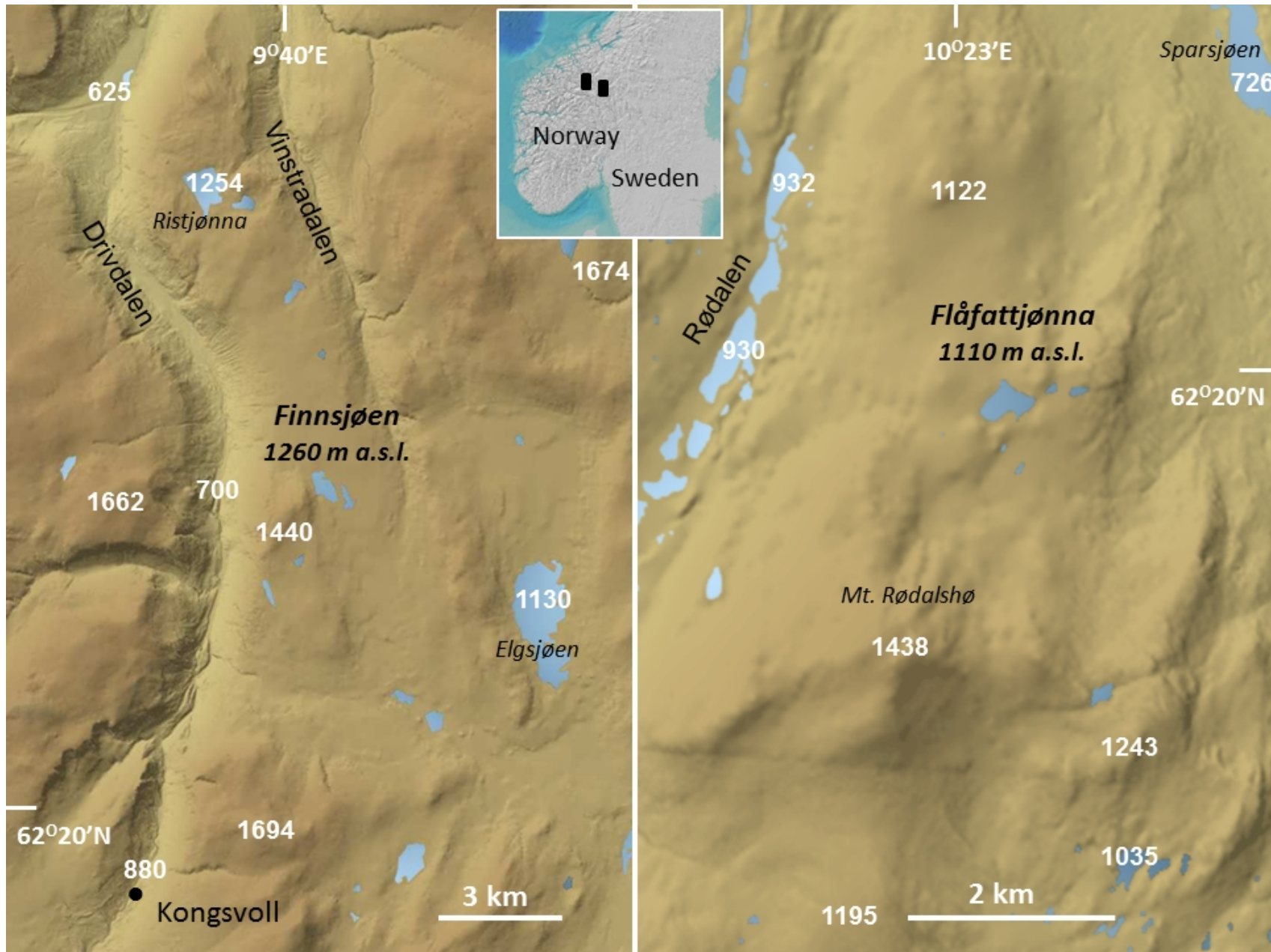
1196 Table 4: Names, dates, and biostratigraphical features of the Finnsjøen local pollen  
1197 assemblage zones (PAZ).

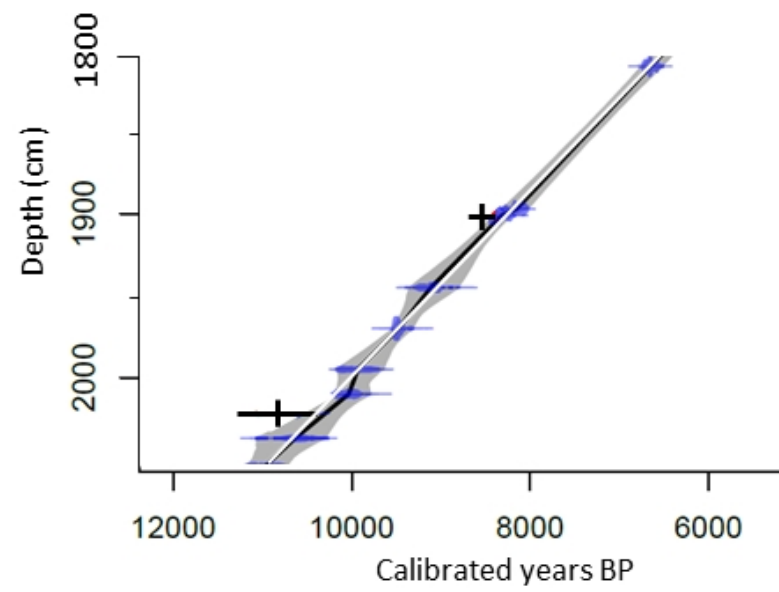




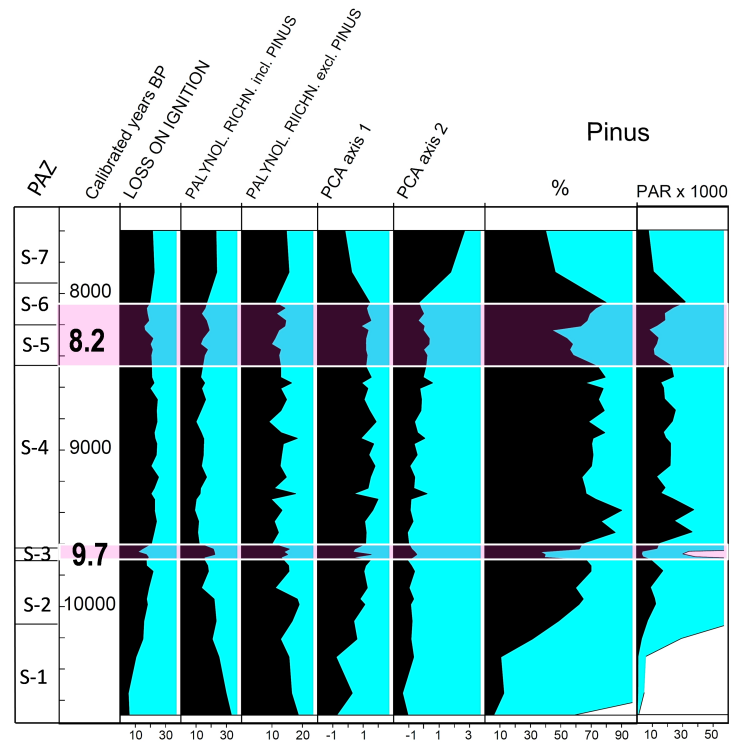


Depth (cm)	$^{14}\text{C}$ Age model	Varve chronology
1865	7600	7600
1876	7800	7806
1888	8000	8015
1899	8200	8226
1910	8400	8433
1922	8600	8641
1933	8800	8847
1944	9000	9048
1956	9200	9250
1967	9400	9450
1978	9600	9648
1990	9800	9842
2001	10000	10038
2012	10200	10227
2024	10400	10424
2035	10600	10619
2040	10700	10717

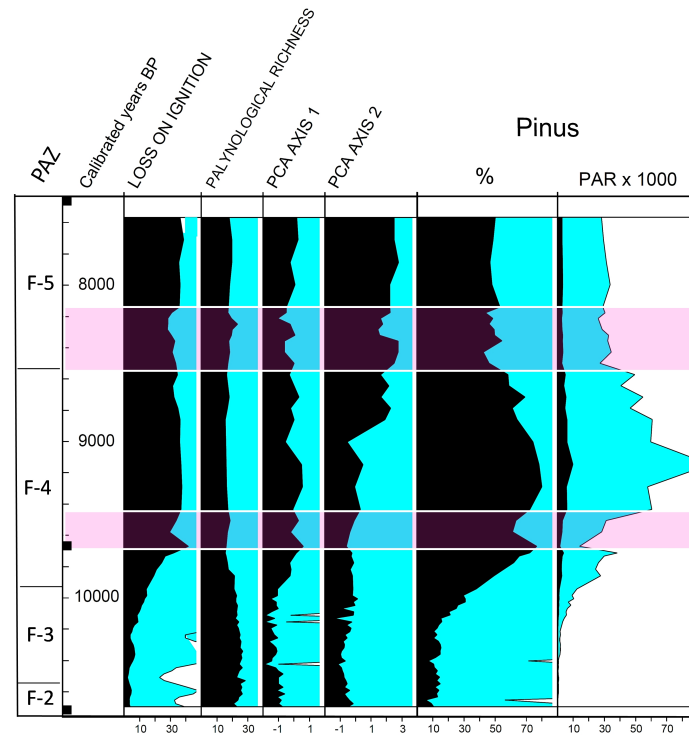




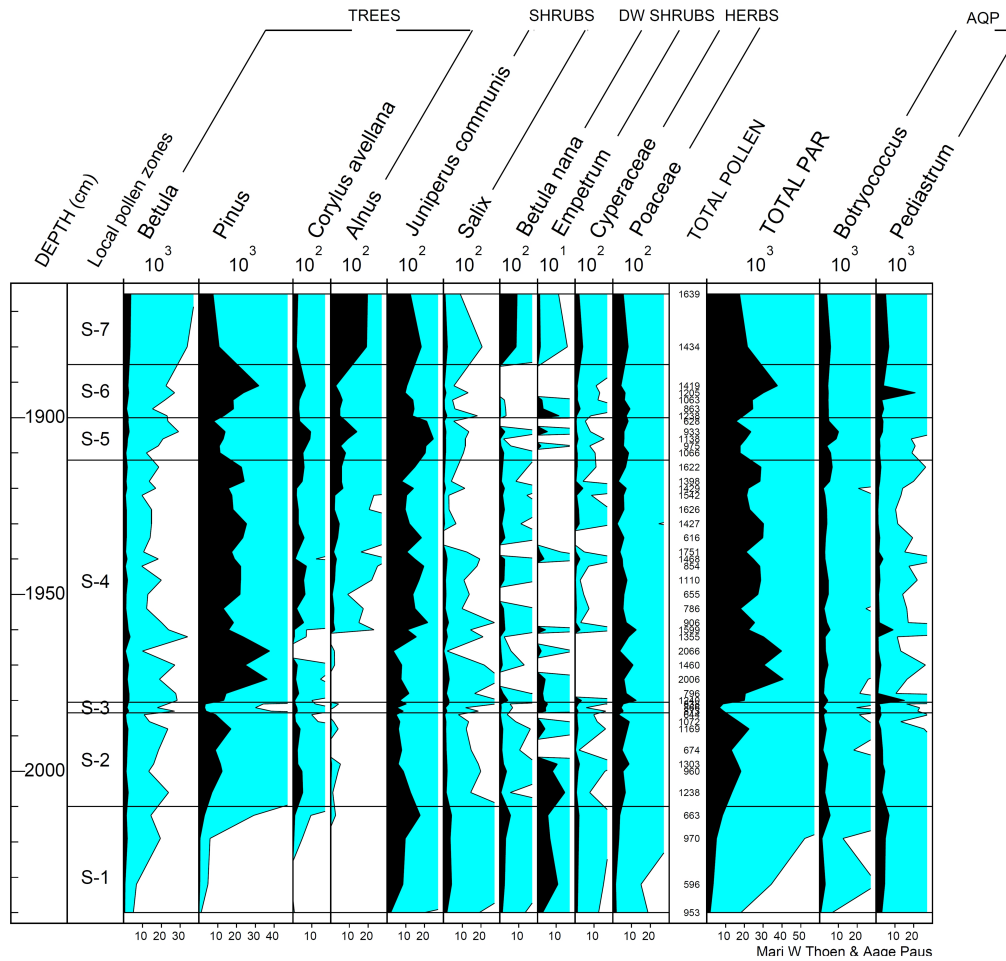
Store Finnsjøen, 1260 m a.s.l.



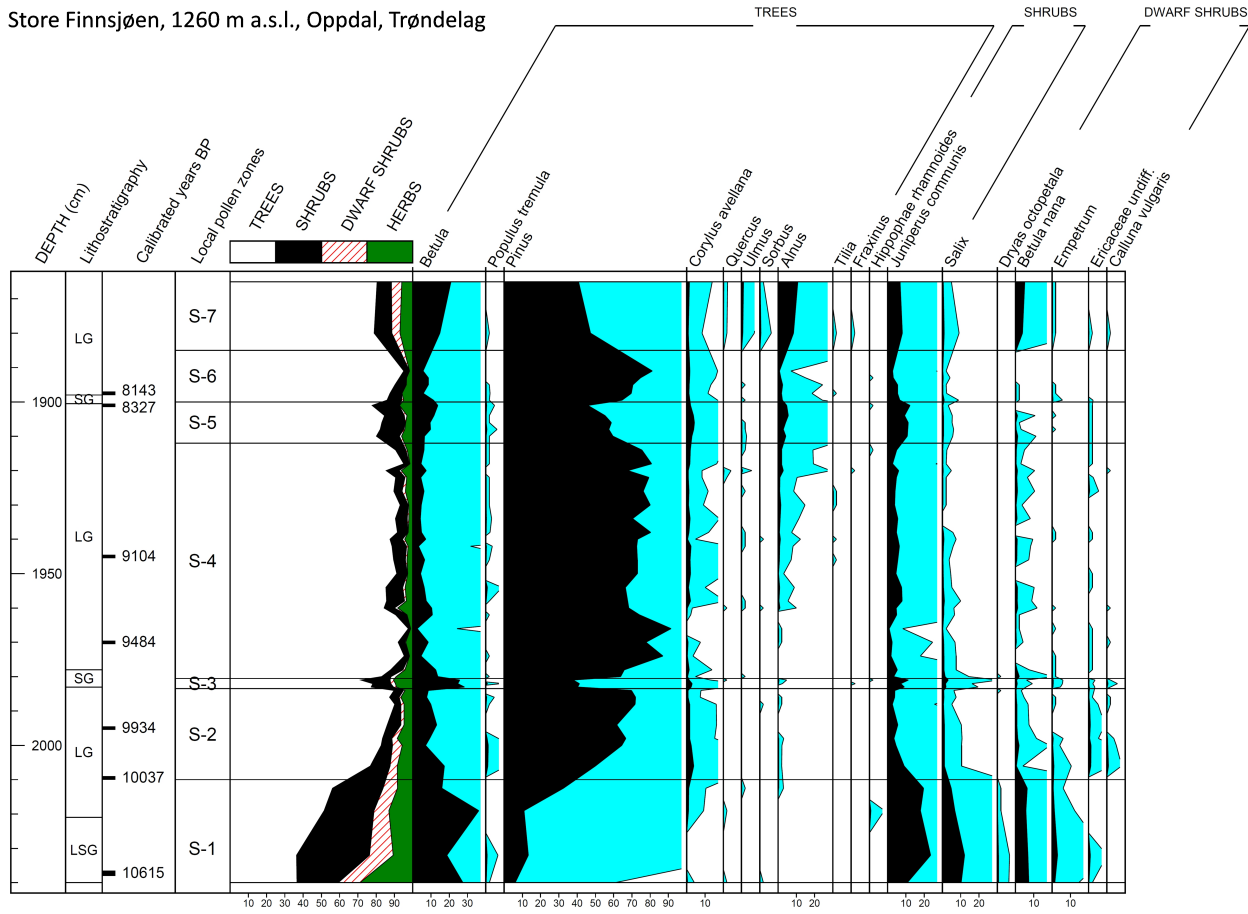
Flåfattjønna, 1110 m a.s.l.

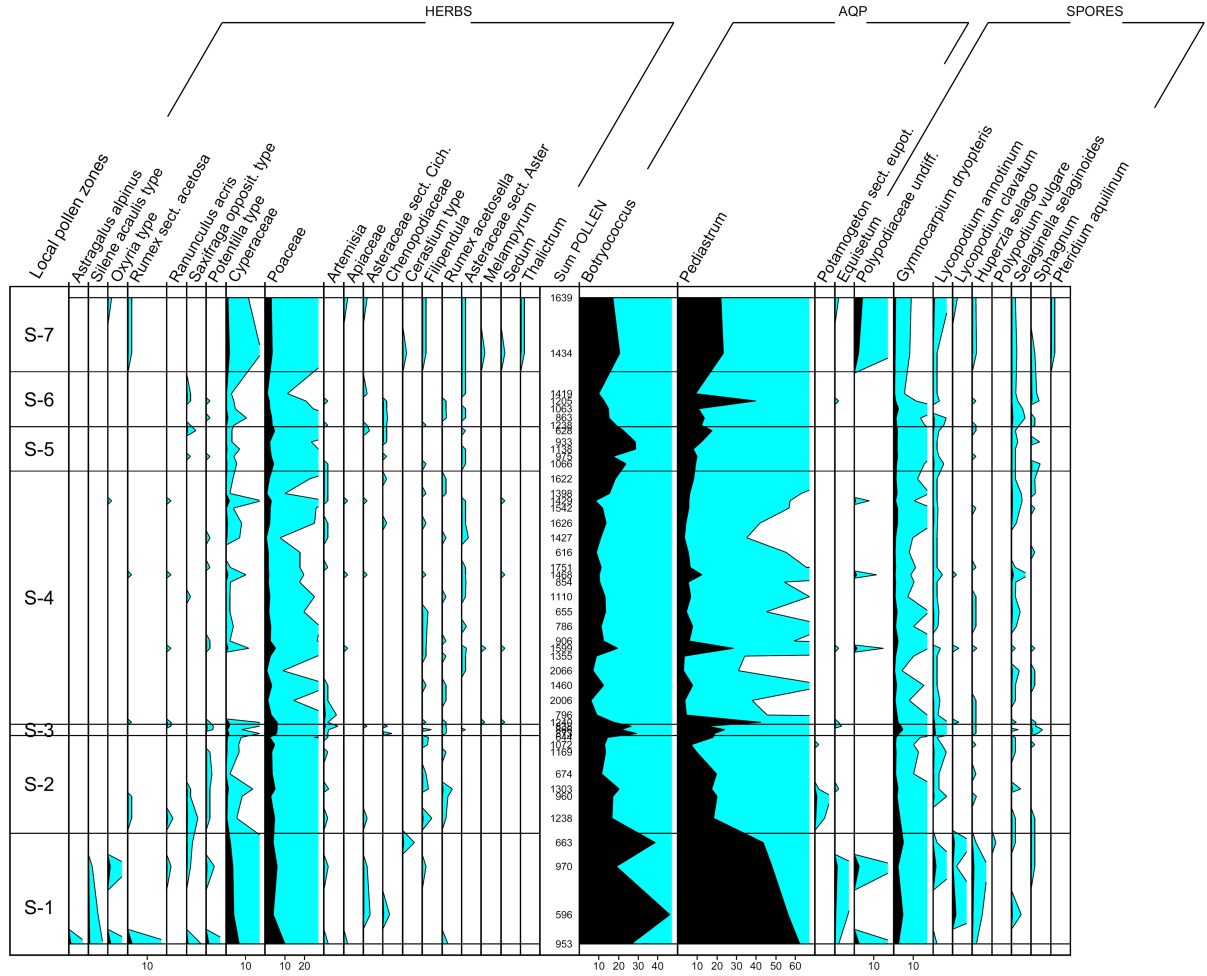


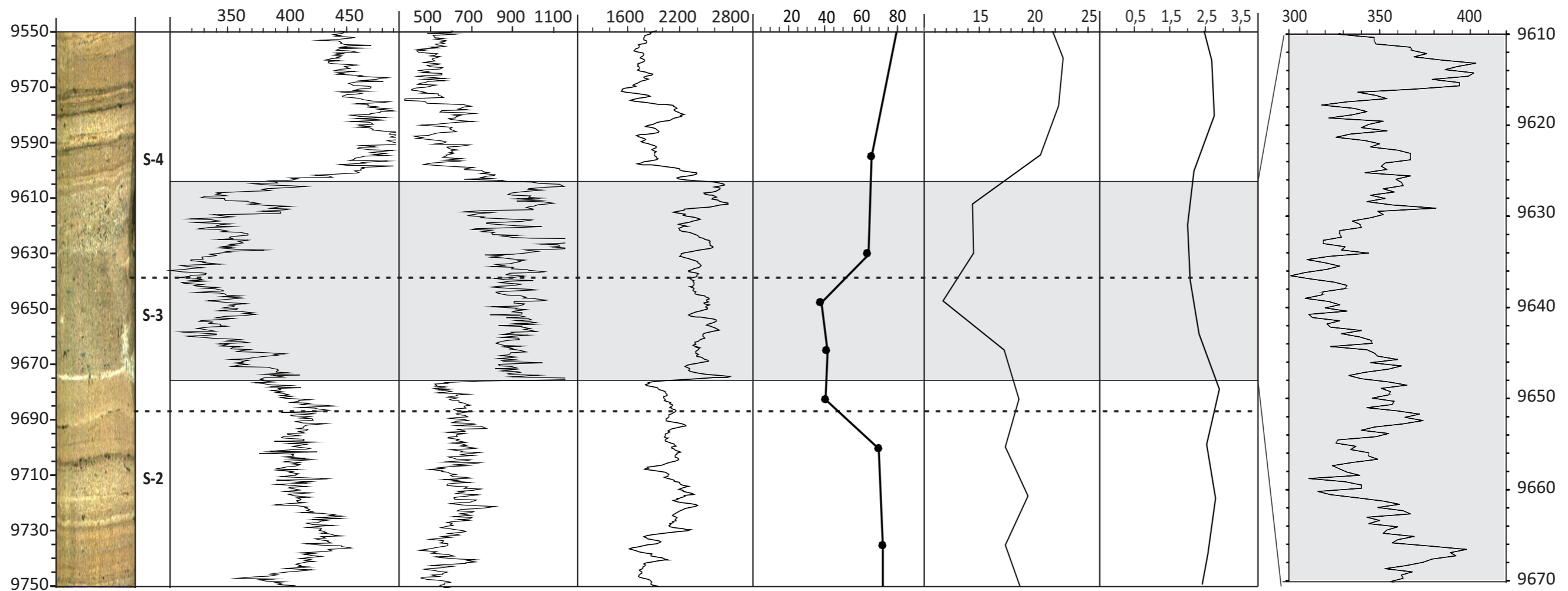
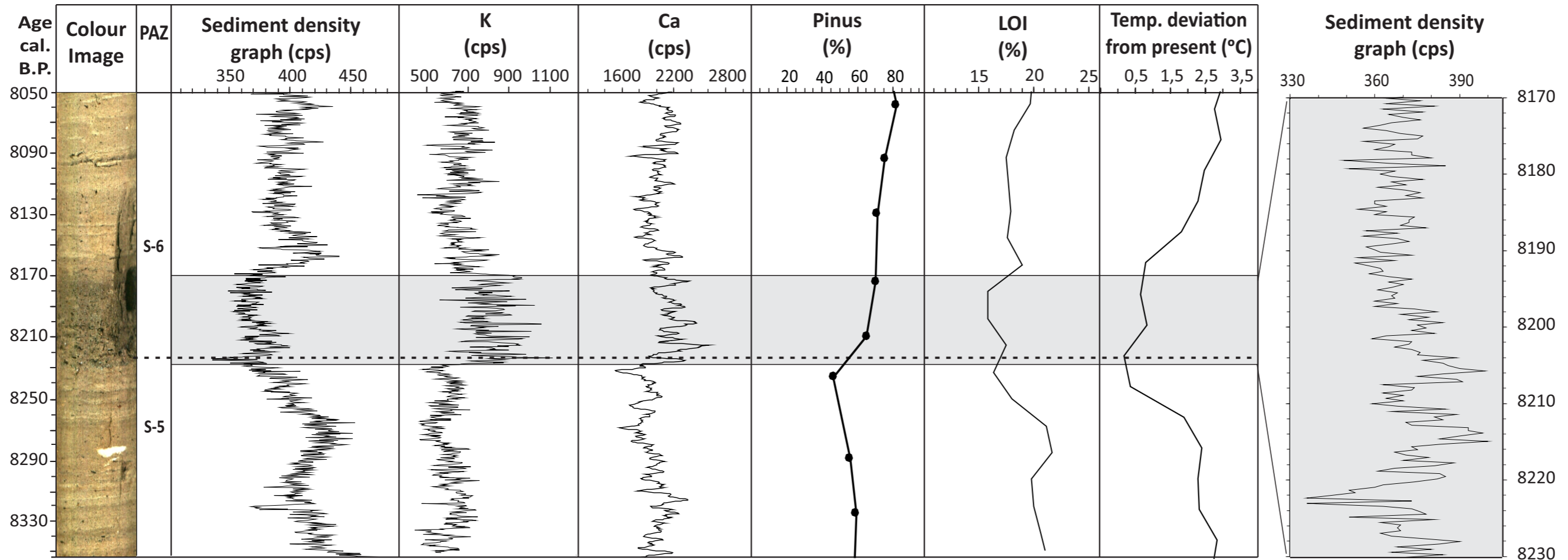
# Store Finnsjøen, 1260 m a.s.l., Oppdal, Trøndelag



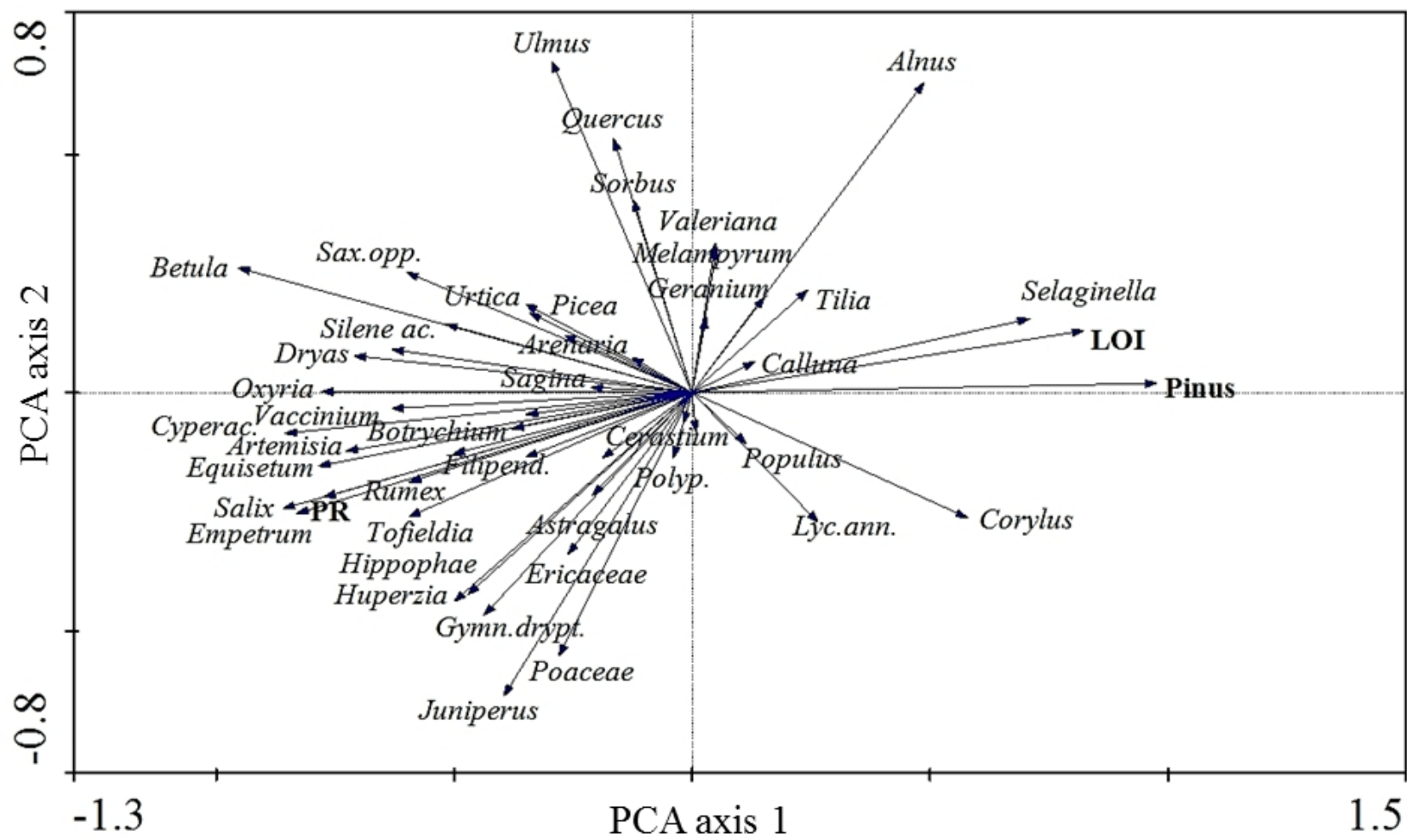
Store Finnsjøen, 1260 m a.s.l., Oppdal, Trøndelag



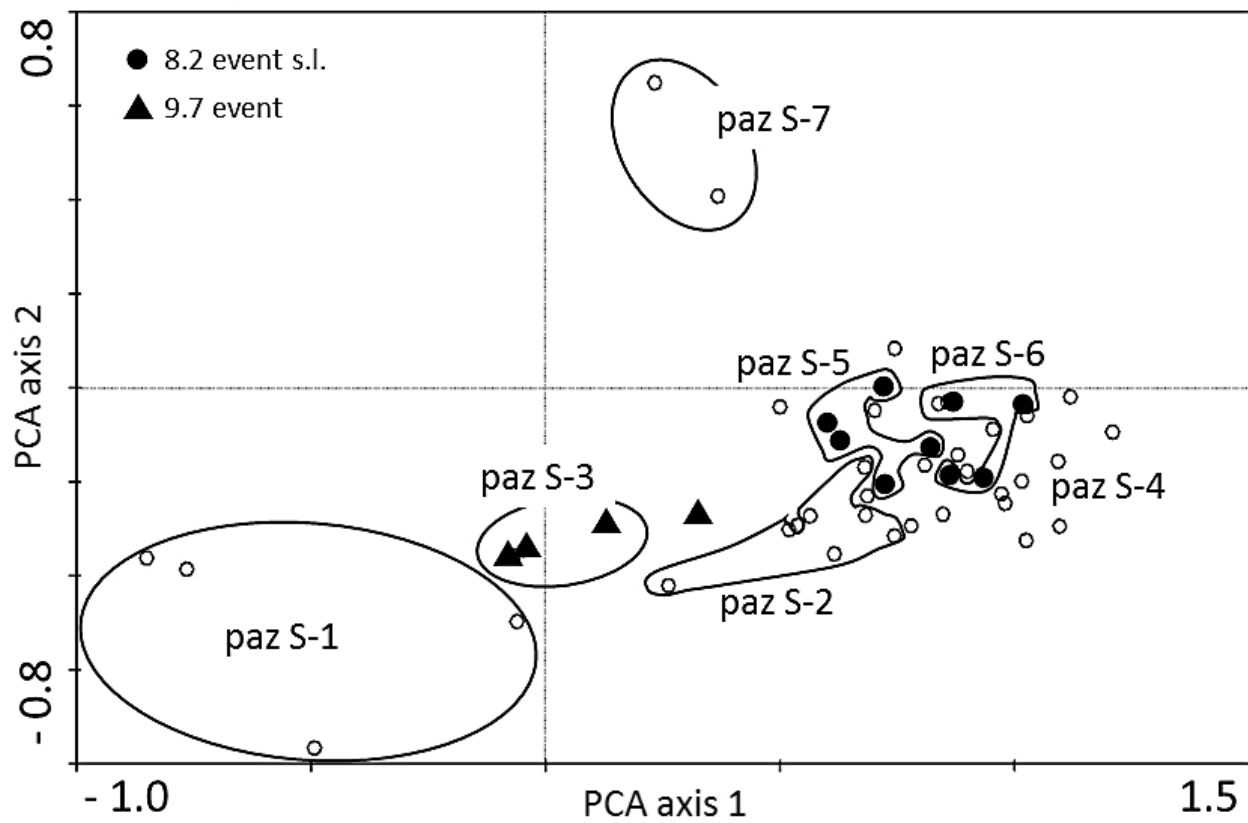








Store Finnsjøen, 1260 m a.s.l.



Flåfattjønna, 1110 m a.s.l.

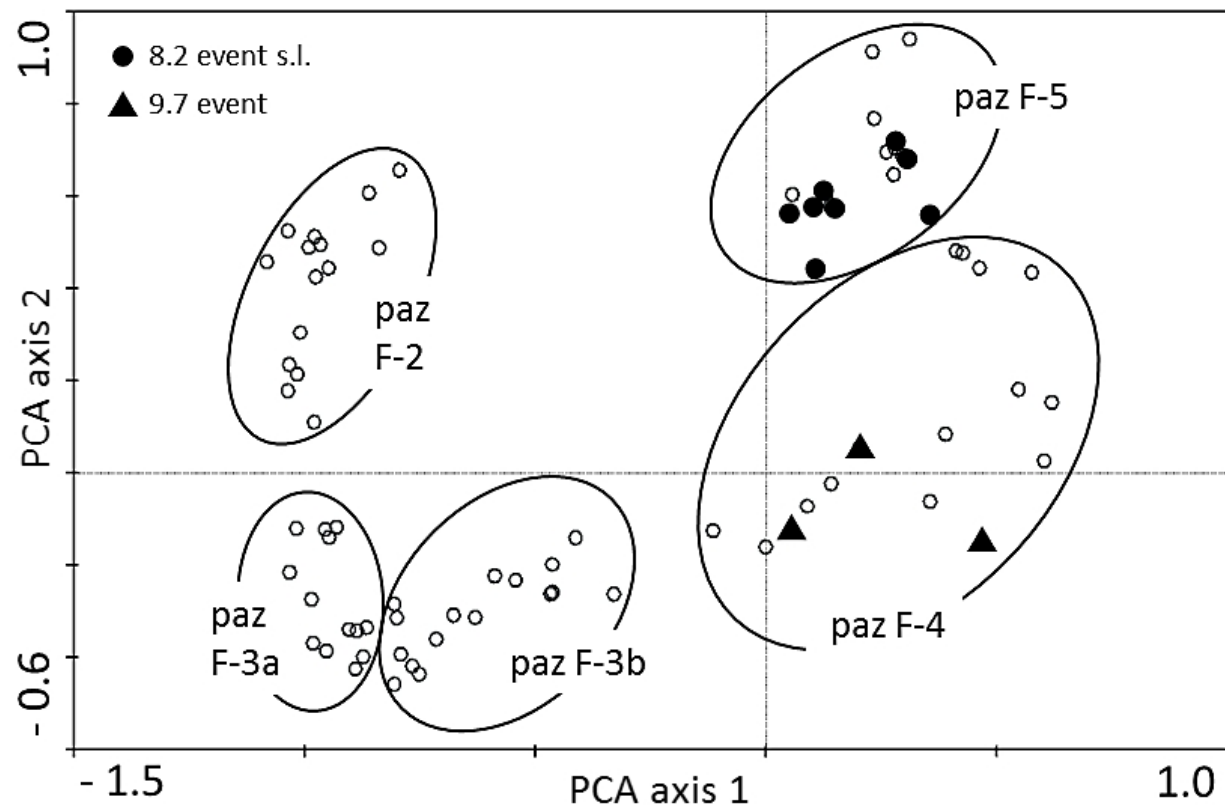


Table 2

<b>Depth (cm)</b>	<b>Description (Troels-Smith 1955)</b>	<b>Colour</b>	<b>Comments</b>
1865-1898	Ld <sup>3</sup> 3, Dh 1, Ag +	Dark brown (nig 3÷)	Laminated gyttja. Less laminated in the upper part. Distinct laminations rich in macrofossils are found at 1893 and 1867 cm. One distinct silty lamina occurs at 1885 cm.
1898-1901	Ld <sup>4</sup> 2, Dh 1, Ag 1	Dark brown (nig 3+)	Silty layer rich in macrofossils and without laminations. Shining from mineral particles.
1901-1978	Ld <sup>3</sup> 4, Dh +, Tb +, Ag +	Dark brown (nig 3)	Laminated gyttja, brown - grey brown in silty laminations. Distinct macro-layers at 1911, 1922, and 1963 cm. Distinct silt layers at 1921, 1929, 1957, 1960, and 1971 cm. One sand lens at 1904 cm
1978-1983	Ld <sup>3</sup> 3, Ag 1	Grey brown (nig 3÷)	Unstratified silty gyttja
1983-2021	Ld <sup>3</sup> 4, Dh +, Tb +, Ag +	Dark brown (nig 3)	Laminated gyttja with macro remains
2021-2040	Ld <sup>2</sup> 2, Dh 1, Ag 1, As +	Brown (nig. 2+)	Laminated clay/silt gyttja. Includes several dark (nig 3) macrofossil-layers less than 1 cm thick. Most distinct between 2021 and 2023 cm (Ld <sup>2</sup> 1, Tb1, Dh1, Ag+). Two mm thick and light (nig 1) clay layer at 2026 cm depth.

Table 3

Lab. Ref.	Depth (cm)	Age (year BP)		$\delta^{13}\text{C}$	Material dated
		Uncal.	Calibrated		
TRa-4463	1810-1811	5840 $\pm$ 45	6505-6747 (6655)	-25.2	Twigs. <i>Salix</i> budscales. Seeds and leaf remains of <i>Betula nana</i> (9.7 mg)
TRa-4464	1897-1898	7340 $\pm$ 55	8019-8310 (8143)	-28.3	Twigs and leaf remains (12.5 mg)
ETH-48538 <sup>A</sup>	1898.5-1900	7658 $\pm$ 31	8395-8537 (8442)	-27.6	Seeds of <i>Betula pubescens</i> and <i>Carex</i> . <i>Dryas</i> leafs. <i>Salix</i> budscales (36.7 mg)
TRa-4465	1900.5-1901.5	7510 $\pm$ 60	8215-8407 (8327)	-26.9	Leaf remains and catkin scales of <i>Betula nana</i> and <i>B. pubescens</i> . <i>Salix</i> budscales. Twigs (23.3 mg)
TRa-4466	1944.5-1945.5	8145 $\pm$ 80	8779-9400 (9104)	-24.7	Seeds and leaf remains of <i>Betula pubescens</i> . Twigs (5.7 mg)
TRa-4467	1969.5-1970.5	8475 $\pm$ 70	9306-9550 (9484)	-26.4	<i>Salix</i> budscales. Leaf remains and twigs (10.6 mg)
TRa-4468*	1994.5-1995.5	8845 $\pm$ 70	9683-10182 (9934)	-27.0	Seeds and leaf remains of <i>Betula pubescens</i> and <i>B. nana</i> . Twigs (16.1 mg)
TRa-4469*	2009-2010	8925 $\pm$ 65	9787-10227 (10037)	-26.4	<i>Salix</i> budscales. Twigs and leaf remains (17.0 mg)
TRa-4470 <sup>A</sup>	2021.5-2023	9450 $\pm$ 75	10503-11081 (10706)	-27.2	Leaf remains of <i>Dryas</i> and <i>Salix polaris</i> . <i>Salix</i> budscales. <i>Carex</i> seeds. Twigs (42.8 mg)
TRa-4471*	2036.5-2038	9380 $\pm$ 115	10258-11076 (10615)	-27.0	<i>Betula nana</i> catkin scales. Leaf remains of <i>Dryas</i> , <i>Salix polaris</i> , <i>B. nana</i> , and <i>Empetrum</i> . <i>Salix</i> budscales. <i>Carex</i> seeds (33.0 mg)
TRa-4472*	2053.5-2055	9620 $\pm$ 85	10723-11200 (10955)	-28.5	Leaf remains of <i>Dryas</i> , <i>Saxifraga sp.</i> , <i>B. nana</i> , and <i>Empetrum</i> . Twigs (26.3 mg)

PAZ	Name	Age (cal. BP)	Pollen zone characteristics	Diagnostic taxa not included in pollen diagrams (Fig. 6)
S-7	<i>Alnus-Betula-Betula nana</i>	7580-7930	Pine declines to 45% $\Sigma$ P and 10 10 <sup>3</sup> grains cm <sup>-2</sup> a <sup>-1</sup> , respectively whereas <i>Alnus</i> , <i>Betula</i> , <i>Ulmus</i> , <i>Betula nana</i> , <i>Juniperus</i> and algae rise. Both palynological richness (PR) and LOI rise.	Rubiaceae, <i>Rubus sp.</i> , <i>Sinapis</i> -type
S-6	<i>Pinus-Betula</i>	7930-8270	Pine percentages rise earlier than pine PAR, both reaching max values (82% $\Sigma$ P, 41 10 <sup>3</sup> grains cm <sup>-2</sup> a <sup>-1</sup> , respectively) in mid S-6. <i>Alnus</i> , <i>Betula</i> , <i>Juniperus</i> and PR show distinct minima. In early S-6, LOI drops to 15% and rises to 24% in late S-6.	
S-5	<i>Alnus-Betula-Juniperus</i>	8270-8520	Pine declines and reaches a minimum (50% $\Sigma$ P, 3 10 <sup>3</sup> grains cm <sup>-2</sup> a <sup>-1</sup> ) in late S-5. <i>Alnus</i> , <i>Betula</i> , <i>Corylus</i> , and juniper show maxima. PAR values for all taxa rapidly drops in late S-5. LOI and PR show no changes from S-4.	
S-4	<i>Pinus-Betula-Populus</i>	8520-9680	Pine strongly rises to its Holocene maximum (90% $\Sigma$ P, 45 10 <sup>3</sup> grains cm <sup>-2</sup> a <sup>-1</sup> ) at 9.4 ka BP, thereafter pine slightly decrease. At 9.4 ka BP, <i>Alnus</i> establishes. In S-4, LOI reaches 20-25%, whereas <i>Betula</i> , <i>Salix</i> , and algae drop to moderate values. PR reaches its Holocene minimum.	<i>Astragalus</i> -t, <i>Campanula</i> , <i>Circium</i> , <i>Euphrasia</i> , <i>Geranium</i> , <i>Geum</i> , <i>Myricaria germanica</i> , Onagraceae
S-3	<i>Betula-Juniperus-Salix</i>	9680-9730	Pine abruptly decreases to 40% and 3 10 <sup>3</sup> grains cm <sup>-2</sup> a <sup>-1</sup> , total PAR reaches a minimum of 7 10 <sup>3</sup> grains cm <sup>-2</sup> a <sup>-1</sup> , and LOI drops to 14%. <i>Betula</i> , <i>Juniperus</i> , <i>Salix</i> , and algae show distinct % maxima, but their PAR values show no changes. PR reaches a maximum of 26.	
S-2	<i>Pinus-Corylus</i>	9730-10,070	Early S-2 shows marked increases in pine (65-70%), LOI (20%), and total PAR (48 10 <sup>3</sup> grains cm <sup>-2</sup> a <sup>-1</sup> ). Tree-birch, juniper, <i>Empetrum</i> , <i>Betula nana</i> , and algae decrease. PAR and PR decrease in the last half of S-2.	<i>Myricaria germanica</i> , <i>Picea abies</i> , <i>Plantago lanceolata</i>
S-1	<i>Betula-Juniperus-Salix</i>	10,070 – 10,670	Sparse pine (< 35 % $\Sigma$ P) and distinct representation of <i>Betula</i> , shrubs/dwarf-shrubs, and algae characterize S-1. Total PAR (< 6 10 <sup>3</sup> grains cm <sup>-2</sup> a <sup>-1</sup> ) and LOI (< 15%) are low. Palynological richness (PR) is high (24-33) and includes many light-demanding pioneer taxa.	<i>Arctous alpinus</i> , <i>Botrychium</i> , <i>Ephedra dist.</i> -t, <i>Euphrasia</i> , <i>Humulus</i> , <i>Myricaria germanica</i> , <i>Picea abies</i> , <i>Polypodium vulgare</i> , <i>Saxifraga hirculus</i> -t, <i>Sax. stellaris</i> -t, <i>Sinapis</i> -t

Table 1

	Lake Finnsjøen (1260 m a.s.l.)	Lake Flåfattjønnna (1110 m a.s.l.)
Geographical position	62°24'N, 9°41'E	62°20'N, 10°24'E
Coring point position UTM 32V NQ	0535133 E 6918753 N	0572506 E 6911883 N
Basin size	800m x 390m	425m x 225m
Basin area	23.7 ha	6 ha
Maximum water depth	14.7 m	13 m
Catchment size incl. basin	69 ha	25 ha
No of inlets /outlets	0 / 1	0 / 1
Local bedrock	greenschists, slate, amphibolite	Phyllite, micashists
July mean	7.5 °C	9 °C
January mean	-11.5 °C	-13 °C
Annual mean	-2.5 °C	-1.5 °C
Annual precipitation	450 mm	500 mm
Local birch-forest line	1100 m a.s.l.	1030 m a.s.l.
Local pine-forest line	900 m a.s.l.	820 m a.s.l.